Cloud Detection Using Satellite Measurements of Infrared and Visible Radiances for ISCCP

WILLIAM B. ROSSOW

NASA Goddard Institute for Space Studies, New York, New York

LEONID C. GARDER

Columbia University, New York, New York

(Manuscript received 10 June 1992, in final form 12 May 1993)

ABSTRACT

The International Satellite Cloud Climatology Project (ISCCP) began in 1983 to collect and analyze weather satellite radiance datasets to produce a new global cloud climatology as part of the World Climate Research Programme. This paper, the first of three, describes the cloud detection part of the ISCCP analysis. Key features of the cloud detection algorithm are 1) use of space and time radiance variation tests over several different space and time domains to account for the global variety of cloudy and clear characteristics, 2) estimation of clear radiance values for every time and place, and 3) use of radiance thresholds that vary with type of surface and climate regime. Design of the detection algorithm was supported by global, multiyear surveys of the statistical behavior of satellite-measured infrared and visible radiances to determine those characteristics that differentiate cloudy and clear scenes and how these characteristics vary among climate regimes. A summary of these statistical results is presented to illustrate how the cloud detection method works in a variety of circumstances. The sensitivity of the results to changing test parameter values is determined to provide a first estimate of the uncertainty of ISCCP cloud amounts. These test results (which exclude polar regions) suggest detection uncertainties of about 10% with possible negative biases of 5% (especially at night).

1. Introduction

The International Satellite Cloud Climatology Project (ISCCP) was established in 1982 as the first project of the World Climate Research Programme (WCRP) to collect and analyze a globally uniform satellite radiance dataset to produce a new cloud climatology (Schiffer and Rossow 1983). Clouds are central phenomena in and provide one link between the two key energy exchange processes that determine earth's climate, namely, solar and terrestrial radiation exchanges and water exchanges. The exchange of radiation at the top of the atmosphere establishes the fundamental constraint on the climate (Lorenz 1967; Hartmann et al. 1986; Peixoto and Oort 1992). Surface observations of cloudiness over the past 20–40 years have served as the primary source of information about clouds [Warren et al. (1986, 1988); see Hughes (1984) for a summary of earlier datasets]. Early estimates of the radiative effects of clouds were based on these surface observations [e.g., London (1957); Manabe and Strickler (1964); see House et al. (1986) for a review], but these early datasets really did not provide enough information about cloud optical properties. Study of cloud microphysics and dynamics has been extensive (e.g., Mason 1971; Hobbs 1974; Twomey 1977; Pruppacher and Klett 1980; Cotton and Anthes 1989) at the scale of individual cloud elements (1–50 km), but this knowledge has yet to be extended to a global description at larger weather system scales that can be used as the basis of simulating clouds in weather and climate general circulation models (GCM). Measurement of cloud properties from satellites can supplement surface observations and in situ studies by extending their results to larger space and time scales and to the whole globe and by obtaining more direct information about cloud radiative properties. Both of these are objectives of ISCCP.

The fundamental measurement made by most satellite instruments is of the intensity of radiation coming from earth with varying spectral discrimination. Instruments on weather satellites have measured radiation in a number of discrete, "narrow" spectral bands to provide imagery of cloud motions and to measure temperature and humidity profiles for use in weather forecasting. To attain the ISCCP objectives, the cloud climatology had to be produced from a satellite dataset that is relatively uniform over the whole globe and over many years, has sufficient time resolution to resolve diurnal variations, has sufficient spatial resolution to

Corresponding author address: William B. Rossow, NASA Goddard Institute of Space Studies, 2880 Broadway, New York, NY 10025.

resolve the most important dynamical scales in the atmosphere, and provides information about the most important cloud radiative properties. In 1982 these criteria were matched most closely by the visible (VIS = 0.65 ± 0.15-μm wavelength) and "window" infrared (IR = 11 ± 1-μm wavelength) imagery from an international suite of weather satellites, both geostationary and polar orbiting. This is still the best match today. The ISCCP collection of a sampled and calibrated version of these data is called the Stage B3 dataset (Schiffer and Rossow 1985).

The design of the cloud analysis for ISCCP is predicated on the desire to obtain enough information about clouds to study how their variations affect the radiation balance and what causes these variations. The limitations of the available satellite data preclude measuring all important properties of clouds, but it is assumed that the most important cloud properties affecting the total radiation balance are also the same properties that are most important in affecting the satellite-measured radiances, namely, cloud amount, cloud-top temperature, and optical thickness (Rossow et al. 1989b). The latter two properties can be related to cloud-top pressure and water content, respectively. To maintain physical consistency, a radiative transfer model is used to relate the satellite radiances to these properties of clouds in the same way that they are related to the complete radiation balance. Isolating the effects of the cloud parameters on the satellite measurements also requires determining and removing the effects of the atmosphere and surface with the same model, so additional sources of information about the atmosphere and surface with compatible coverage and resolution are needed. By combining the data describing the atmosphere and surface with the satellite cloud analysis into one physically consistent model, enough information is made available (Rossow and Schiffer 1991) to calculate the separate effects of clouds, atmosphere, and surface on the radiation balance and to examine the relations of cloud property variations to standard meteorological information (cf. Rossow and Lacis 1990).

The subject of this paper is the method by which the ISCCP satellite observations are separated into "clear" and "cloudy" categories, commonly called "cloud detection" (Rossow 1989). Key objectives are to examine the statistical variations of observed radiances to understand the meaning of "clear" and "cloudy" and the significance of variations in the number of locations that are "cloudy." Section 2 of this paper describes the data analyzed, while section 3 describes the steps in the cloud detection algorithm. Section 4 presents the radiance statistics that were used to test the selection of particular algorithm steps and illustrates the sensitivity of the results to the selected test parameter values. The most important "new" feature of the ISCCP analysis is testing for time variations [see Sèze and Rossow (1991a) for a more extensive treatment]. Section 5 summarizes the paper.

Two companion papers present results from extensive validation studies. Since clouds are identified by radiances that differ from values representing clear conditions, validation of cloud *detections* is provided by confirming the accuracy of the clear radiance values (cf. Rossow et al. 1989b). Since the atmosphere is nearly transparent at VIS and IR wavelengths, clear radiances are determined primarily by the properties of the surface (visible reflectance and brightness temperature, respectively) for which several other independent or related measurements exist. The accuracies of the ISCCP values of surface reflectance and temperature are assessed in the first companion paper (Rossow and Garder 1993). Having determined the presence or absence of clouds at each location and time, we can define a cloud amount that can be validated by comparison with other measurements of similar quantities (Rossow et al. 1993). Also presented in the second companion paper is a comparison of the ISCCP cloud amount climatology with three other cloud climatologies, two from satellite and one from surface observations.

2. Data

The primary measurements are of the time/space distributions and variations of reflected visible (VIS) and emitted infrared (IR) radiation from earth observed by a suite of satellite-borne imaging radiometers. Since many parts of the earth atmosphere–surface system affect these radiances, the ISCCP analysis combines these satellite radiances with other data that describe some of the properties of the atmosphere and surface to isolate the contributions of clouds. In effect, the analysis finds the combination of cloud, atmosphere, and surface properties that, when used in a radiative transfer model, matches the satellite measurements.

a. ISCCP stage B3 data

The satellite radiance data come from operational weather satellites: the geostationary satellites provide high time-resolution images of lower latitudes over a limited longitude range and the polar orbiters provide global coverage with lower time resolution. The satellites that have provided data from 1 July 1983 to date are 1) *Meteosat-2, Meteosat-3, Meteosat-4,* and *Meteosat-5,* operated by the European Space Agency; 2) *GMS-1, GMS-2, GMS-3,* and *GMS-4,* operated by the Japan Meteorological Agency; 3) *GOES-5, GOES-6,* and *GOES-7,* operated by the U.S. National Oceanic and Atmospheric Administration (NOAA), and 4) *NOAA-7, NOAA-8, NOAA-9, NOAA-10, NOAA-11,* and *NOAA-12,* operated by NOAA. Each geostationary satellite covers about 120° of longitude for about ±60° of latitude: Meteosat covers 60°W to 60°E, GMS cov-

ers 80°E to 160°W, GOES-West covers 165°E to 75°W, and GOES-East covers 135°W to 15°W. The polar-orbiting satellites each observe all lower latitudes twice daily and provide coverage of the regions poleward of about 50° at somewhat higher frequency.

These radiance data are collected by sector processing centers (SPC—listed in appendix A). Data volume is reduced in three steps: time sampling, reduction of the resolution of the VIS data to match the IR data (if necessary), and spatial sampling. The geostationary observations, taken as frequently as every 30 min, are sampled once every 3 h; the polar orbiter data are not sampled in time. Most satellites have smaller instrument fields of view (FOV) for measurements made at solar wavelengths than at thermal infrared wavelengths; for these satellites the solar radiances are averaged to match the infrared spatial resolution, producing a spatial resolution of 4–7 km. Finally, the measurements in individual FOVs (called pixels) are sampled to a spacing of about 24–30 km.

The precision of the radiance measurements, expressed as the number of binary digits (bits) used to represent the measurement, ranges from 6–10 for VIS and 8–10 for IR; however, the averaging of some VIS data to reduce its spatial resolution improves its precision somewhat, whereas noise levels in some instruments limit precision. Thus, all radiances are represented by 8 bits, a precision of about 0.4%.

These radiance data are collected at the Global Processing Center (Appendix), quality inspected, calibrated, navigated and reformatted to produce the ISCCP stage B3 dataset (Schiffer and Rossow 1985; Rossow et al. 1987). The radiance calibration procedure consists of four steps: 1) application of the nominal calibration supplied by the satellite operator, 2) comparison of all geostationary radiometers to the underflying polar orbiter to normalize all radiances to the current polar orbiter (Desormeaux et al. 1993), 3) correction of short-term calibration anomalies (Desormeaux et al. 1993), and 4) normalization of all polar orbiters to a single reference (*NOAA-7*) and correction of polar orbiter calibrations for instrument drift (Brest and Rossow 1992).

Subsequent to the processing of the stage B3 data, a much better absolute calibration was obtained for the VIS channels on the polar orbiters (Whitlock et al. 1990), requiring the following correction of all VIS radiance values on stage B3 data tapes:

multiply B3-VIS by 1.2.

We process one month of data from an individual satellite at one time. In the ISCCP detection algorithm, the effects of diurnal variations (as well as of varying satellite viewing and solar illumination geometries) are minimized by comparing radiance variations in time at constant diurnal phases. For geosynchronous satellites and high-latitude polar orbiter data, this is accomplished by sorting the images according to one of eight nominal UTC (0000, 0300, 0600 . . .). Since observations from a sun-synchronous polar orbiter have nearly constant diurnal phases at lower latitudes, these data are composited into one "daytime" and one "nighttime" image for each day.

To compare the time variations of radiance values at each location, individual image pixels must be earth located. Since the earth location of each image pixel varies with time (due to relative motions of the satellite and earth), the spatial sampling used to select the ISCCP B3 radiance data limits the precision with which they can be collocated. Moreover, the accuracy of the available navigation is also limited (Rossow et al. 1987). Although the satellite FOVs represent areas on the surface of earth ranging in size from 4 to 7 km, we map the ISCCP B3 pixels to a grid with a spatial resolution of about 25 km and treat the radiances as representative of conditions in this larger-sized area. (Henceforth, "scene" refers to these map cells, which have constant locations.) This approach produces some additional variation of the radiances under clear conditions, since the properties of surface are not constant with location, but Sèze and Rossow (1991a) show that the magnitude of the variations at scales less than 50–100 km is very small compared with the time variations.

The effects on the radiances of small variations of satellite viewing and solar illumination geometries are reduced during the mapping step by application of approximate (reversible) corrections for their angular dependence. All IR radiances are corrected to an approximate nadir view by using a satellite zenith angle dependence calculated with the same radiative transfer model used to analyze the data, together with zonal, monthly mean atmospheric conditions taken from the TOVS data.[1] All VIS radiances are converted to reflectances by dividing by the cosine of solar zenith angle. Once clear VIS and IR values are selected, the reverse corrections are applied to reconstruct the appropriate angular dependence for each scene and time.

b. NAVY/NOAA ice/snow data

The cloud detection analysis is aided by additional information identifying the presence of sea ice and snow cover in the scene. This information is obtained from two operational data products, the U.S. Navy/NOAA Sea Ice Product and the NOAA Snow Data Product [see appendix B in Rossow et al. (1991)]. The former provides weekly reports of fractional sea ice coverage at a spatial resolution of about 18 km. The latter provides weekly reports of snow presence or absence (if a grid cell is judged to be more than 50%

[1] NOAA TIROS Operational Vertical Sounder data products contain profiles of atmospheric temperature and precipitable water vapor amount, plus total ozone abundances [see appendix A in Rossow et al. (1991)].

covered, then snow is reported) at a spatial resolution of about 150–200 km. These two datasets are combined into a common dataset with a resolution of about 100 km and a 5-day time interval for use in the analysis.

c. *Other ancillary data*

Three other datasets are used to classify each location on earth by surface type. Each latitude–longitude is identified as land, water, or coast (mixture of land and water) at 0.25° resolution, based on a dataset derived from Masaki (1976). The mean surface topographic altitude and "roughness" are determined from a topography dataset distributed by the National Geophysical Data Center in Boulder, Colorado. These data have a resolution of at least 10′ latitude–longitude (about 20 km), which is reduced to 0.25° resolution. The "roughness" is determined by the range of topography reported within a 400 × 400 km region surrounding each 0.25° map cell. The land/water and topography datasets have been edited to eliminate contradictions (e.g., mountains on water, some associated with small islands, some representing errors); the land/water data have also been compared to the snow/ice data to eliminate contradictions (snow on water and sea ice on land). Finally, each land area is classified according to the type of vegetative cover using the data of Matthews (1983, 1984).

These datasets, together with the sea ice/snow datasets, divide the surface into the following categories. For IR properties the categories are open water, water near coasts or covered by sea ice, low-lying land, and land with rough terrain, high topography, or permanent ice cover. For VIS properties the categories are open water or dense vegetation (all forests, woodlands), sparse vegetation types, deserts, or high topography, and sea ice–covered water, or snow-covered land.

3. Description of algorithm

a. *Overview*

Selection of an algorithm for ISCCP began in 1982 with a comparison of several methods, including simple and complex threshold methods and several statistical methods, all applied to the same dataset (Rossow et al. 1985). All methods produced similar results for total cloud amount: the spatial correlations between methods were >0.7, the biases between methods were typically <10%–15%, and the scatter of results was about 15%–20% rms. Closer examination of the comparison results (Rossow et al. 1985) suggested four key conclusions. 1) About two-thirds of the clouds produced such large and rapid variations of IR and VIS radiances that they were successfully detected by all methods. 2) The largest differences between the methods occurred in areas where the surface properties varied rapidly in time (e.g., snow-covered land), or over small spatial scales [e.g., coastlines—see Saunders (1986), Sèze and Desbois (1987)], or in areas where a significant portion of the clouds were either very low level and broken [e.g., fair weather or trade-wind cumulus—Coakley and Baldwin (1984)] or optically very thin (e.g., cirrus). 3) If ways could be found to increase the accuracy of the clear radiances, then all of the algorithms could be made more sensitive to the presence of clouds in low-contrast situations. 4) The diversity of conditions encountered on earth precludes the use of any one method everywhere. A successful global cloud algorithm must be situation dependent and employ a series of tests to retain flexibility (cf. Coakley and Baldwin 1984; Rossow et al. 1985; Saunders 1986; Saunders and Kriebel 1988; Rossow et al. 1989b; Key and Barry 1989). This approach is a departure from earlier, context-independent methods, which are closer to classical pattern recognition techniques.

In the comparison tests, use of the statistics of spatial variability to detect clouds in single images did not seem effective in complex regions, such as coastlines (cf. Desbois and Sèze 1984; Saunders 1986). Subsequent research has focused on use of time variations to identify clear conditions (Coakley and Baldwin 1984; Desbois and Sèze 1984; Gutman et al. 1987; Sèze and Desbois 1987; Rossow et al. 1989b; Sèze and Rossow 1991a).

Casual visual examination of radiance images shows numerous cloud features that appear to be quite distinct from the cloud-free portions of the image. However, this impression is produced by the common practice of enhancing photographic contrast. In fact, the frequency distribution of image radiances, when displayed in the form of one- or two-dimensional histograms, forms a continuum from "clear" values to "cloudy" values. This continuity is observed at all space and time scales (cf. Kuo et al. 1988; Welch et al. 1988; Rossow 1989; Sèze and Rossow 1991a; Wielicki and Parker 1992). Thus, cloud detection requires dividing the radiance data into a group of image pixels with a high probability of being cloud affected and a group that is either totally cloud-free or "barely" cloud affected (Rossow 1989). This decision can be expressed as a threshold statement: a pixel is termed cloudy only if at least one radiance value is distinct from the inferred clear value at a given place/time by an amount larger than the uncertainty in that clear value caused by measurement errors and the natural variability of clear conditions. This approach minimizes false cloud detections, but can still miss clouds that resemble clear conditions at all available wavelengths.

The design of the ISCCP cloud algorithm is governed by the primary scientific goal of the project, which is to determine the role of cloud–radiation interactions in the climate (Schiffer and Rossow 1983). Since low-level and cirrus clouds may play crucial roles in determining global cloud radiative feedbacks, the detection sensitivity of the cloud algorithm must be maximized. The key to the success of threshold methods lies in

how accurately the reference (clear sky) value is selected, so most of the algorithm is devoted to this task. If clear radiance values are obtained from another source, the cloud detection can be simple, as is the case with the method used by Stowe et al. (1988), for example. However, it is misleading to think of the ISCCP method as simply a "constant threshold test" because of the situation dependence of the radiance analysis. The validity of the cloud detection must be judged primarily by the accuracy of the clear radiances (see Rossow and Garder 1993). The ISCCP cloud-detection algorithm consists of five steps (Rossow et al. 1991). A guide to the algorithm steps and their description is as follows.

1) Space contrast test (applied to individual IR images)	part b1	equation (1)	Table 1	—
2) Time contrast test (three consecutive IR images at constant diurnal phase)	part b2	equation (2)	Tables 1 and 2	Fig. 1a
3) Cumulation of space/time statistics (both IR and VIS images)	part c	—	—	—
4) Construction of clear-sky composites (both IR and VIS once every 5 days at each diurnal phase and location)	part d	—	Table 3	Fig. 2
5) Radiance thresholds (both IR and VIS images)	part e	equation (3)	Table 4	Fig. 3

b. Pixel classifications

1) SPACE CONTRAST TEST

Examination of spatial variations of IR and VIS radiances at one instant of time reveals four sources of variation, in order of decreasing magnitude (cf. Sèze and Rossow 1991a): 1) mixtures of cloudy and clear areas, 2) changes of cloud properties with location in a completely overcast area, 3) changes of surface properties with location in a uniformly clear area, and 4) changes of atmospheric properties with location. This ranking is not universal, although at the particular wavelengths we use, atmospheric changes generally have the smallest effect. Examples where the change of surface properties are the largest source of variation are the Sahara desert and its coastline in VIS. An example where the change of cloud properties is the largest source of variation is marine stratus clouds in VIS (cf. Sèze and Rossow 1991a,b).

A number of studies have illustrated the generally lower spatial variability associated with clear conditions and have used spatial variability of infrared and/or visible radiances as a way to detect clouds. Examples are the spatial variance method (Coakley and Bretherton 1982; Coakley and Baldwin 1984) and radiance histogram "clustering" techniques (Simmer et al. 1982; Desbois and Sèze 1984; Arking and Childs 1985). In the first ISCCP algorithm step, a spatial variability test is applied only to IR radiances (since these are expressed as brightness temperatures, we will refer to them as temperatures, T) in the original image coordinates. The tendency for cloudy conditions to be colder than clear conditions and to exhibit more spatial variability is tested for by selecting the largest IR brightness temperature, T_{MAX}, in a small region and comparing this value to those in all neighboring pixels, T_i:

$$\text{cloudy:} \quad T_i < (T_{MAX} - \text{DELTA1})$$

$$\text{undecided:} \quad T_i \geq (T_{MAX} - \text{DELTA1}), \quad (1)$$

where DELTA1 is the contrast threshold (Table 1).

In order for this simple test to work with sufficient reliability, several factors must be carefully controlled. 1) The land/water class of all pixels within a region must be identical, otherwise the inherent contrast between land and ocean surface radiances would dominate the results. All coastal regions with mixed land and water pixels are excluded from the spatial contrast test. 2) The size of the regions must be properly chosen. If a region is too small, the probability of large contrast indicating cloud-affected pixels is much smaller; if a region is too large, there is an increased likelihood of false detections due to larger spatial variations of the surface conditions. 3) The shape of the selected regions is also important, since there are stronger meridional than zonal gradients in surface temperature. Moreover,

TABLE 1. Numerical values used in the IR space and time contrast tests.

Surface type	Spatial domain	DELTA1	Time domain	DELTA2	DELTA3
Ocean	15 × 15 (450 km × 450 km)	3.5 K	1 day	1.1 K	3.5 K
Ice-covered water	3 × 3 (90 km × 90 km)	6.5 K	1 day	2.5 K	8.0 K
Land	3 × 3 (90 km × 90 km)	6.5 K	1 day	2.5 K	8.0 K

the meridional gradients are larger at higher latitudes, an effect that is exacerbated by viewing zenith angle variations in geostationary satellite images. To reduce the magnitude of these effects, we construct an ocean grid by defining subregions in the original, sampled image coordinates with varying dimensions, from 15 pixels by 15 scan lines near the equator to 25 pixels by 9 scan lines near the earth's limb in geostationary satellite images and at higher latitudes in polar orbiter views. The land grid is small enough, 3 pixels by 3 scan lines, that this effect can be neglected. 4) The size of the contrast threshold, DELTA1, must be larger than the magnitude of natural variations associated with the surface and clear atmosphere and smaller than that caused by clouds. Too low values of DELTA1 cause an increased likelihood of misidentification due to the natural variability of surfaces, leaving too few clear values for meaningful statistics. Too high values of DELTA1 cause the number of cloud detections to decrease and increases the likelihood of contamination of the clear values. These two criteria can conflict (i.e., cloud variability may be as low as surface variability), but our objective is to identify clear conditions reliably, so we select small values of DELTA1 to minimize cloud contamination of clear radiances. The fact that the pixel with $T_i = T_{MAX}$ is labeled undecided in Eq. (1) is what makes this primarily a test for spatial variability, since for a single image we do not know whether the warmest pixel is clear. The values used in the spatial contrast test are given in Table 1 and are different for land and ocean because of the differences in the variability of both cloudy and clear conditions encountered (see section 4).

2) TIME CONTRAST TEST

Examination of time records of IR and VIS radiances at individual locations reveals four kinds of variation, in decreasing order of magnitude (cf. Sèze and Rossow 1991a): 1) variations due to formation/dissipation of clouds or to movement of clouds into or out of an area, 2) quasi-periodic variations associated with the diurnal heating and cooling cycle (IR) or with changes in the solar illumination (VIS), 3) variations of surface conditions at synoptic and seasonal time scales, and 4) variations caused by changes in atmospheric conditions. This ranking is nearly universal, but there are important exceptions. The daily variation of solar illumination usually causes larger changes in VIS than caused by the occurrence of cloud. The diurnal variation of land surface temperatures in the tropics can be larger than the effect of boundary-layer cloudiness on IR radiances.

A number of studies have shown that the temporal variability of radiances caused by clouds is generally larger than the spatial variability, particularly at solar wavelengths, and have developed simple tests for cloud detection (Shenk and Curran 1973; Reynolds and Vonder Haar 1977; Minnis and Harrison 1984; Gutman et al. 1987; Sèze and Desbois 1987; Rossow et al. 1989b). The key difficulty in separating cloudy and clear situations using the time variations of the radiances is that the diurnal variation of solar illumination and of surface temperature, particularly on land, can be large enough to preclude a sensitive test. Minnis and Harrison (1984) resolved this problem by modeling the effects of varying solar illumination and of the full diurnal cycle of surface temperatures anchored on the clear values identified in daytime tests of VIS data. The ISCCP analysis examines time variations at constant diurnal phase to minimize the influence of diurnal variations.

The time contrast test involves three time-consecutive images (labeled "yesterday" = −1, "today" = 0, and "tomorrow" = +1) at a given UTC. Every image in a time sequence is tested as the "today" image (the first and last image in each month have only one time test result). The IR brightness temperature in a scene, T_j, is compared to the value in the same scene on the previous day, T_{j-1}, and following day, T_{j+1}. Each scene is labeled by the magnitude of the radiance difference in three ranges (also for $T_j - T_{j+1}$):

$$\left.\begin{array}{ll} \text{clear:} & |T_j - T_{j-1}| < \text{DELTA2} \\ \text{undecided:} & \text{DELTA2} \leqslant |T_j - T_{j-1}| \leqslant \text{DELTA3} \\ \text{cloudy:} & |T_j - T_{j-1}| > \text{DELTA3 and } T_j < T_{j-1} \end{array}\right\} \quad (2)$$

where DELTA2 < DELTA3 are contrast thresholds (Table 1). The combined logic table for the "yesterday" and "tomorrow" tests is shown in Fig. 1a.

In order for this simple test to work with sufficient reliability, several factors must be considered. 1) If the smaller threshold (DELTA2) is smaller than the natural variability of the surface, then the number of clear radiance values identified will be too few for meaningful statistical tests. 2) If the smaller threshold is too large, low-level broken cloudiness, which does not alter the IR radiances very much, will be mistaken for clear conditions (this sometimes happens anyway, see section 4). 3) If the larger threshold (DELTA3) is too small, the number of scenes identified as clear is also reduced because more disagreements between the "yesterday" and "tomorrow" test will occur. Moreover, rarer events associated with large storms that involve larger changes of the surface temperature can be mistaken for cloudy situations, which would bias the statistics of the natural variation of clear conditions. Numerical values used in the time contrast test are given in Table 1 and are different for land and ocean because of the differences in the variability of both cloudy and clear conditions encountered (see section 4).

3) JOINT CLASSIFICATION

The first two steps of the ISCCP cloud detection algorithm are combined to classify IR radiances into one

TIME TEST LOGIC

TOMORROW'S TEST \ YESTERDAY'S TEST	CLOUDY	UNDECIDED	CLEAR
CLOUDY	CLOUDY	CLOUDY	MIXED
UNDECIDED	CLOUDY	UNDECIDED	CLEAR
CLEAR	MIXED	CLEAR	CLEAR

COMBINED SPACE-TIME TESTS LOGIC

TIME TEST \ SPACE TEST	CLOUDY	UNDECIDED
CLOUDY	CLOUDY	CLOUDY
UNDECIDED	CLOUDY	UNDECIDED
MIXED	MIXED	MIXED
CLEAR	MIXED	CLEAR

FIG. 1. Logic tables (a) to combine the results of the time contrast test comparing the "today" image with the "yesterday" and "tomorrow" images and (b) to combine the results of the space contrast test and the time contrast test. Undecided means that no decision (cloudy or clear) is made for a particular scene. Mixed indicates contradictory decisions by different tests. All comparisons are performed separately for each diurnal phase.

of four classes: probably cloudy, probably clear, indeterminate, and mixed. The last two classes contain scenes that were ambiguous in all tests or had strongly contradictory results, respectively. The logic is illustrated in Fig. 1b.

The classification steps are designed to obtain "high quality" statistics about clear radiances. Thus, the tests for the presence of cloud are made so strict that some values that might represent clear conditions are discarded to be sure of eliminating all of the significant cloud effects, as one might do in a "cloud clearing" algorithm for surface studies [cf. discussions in Pinty and Szejwach (1985); Saunders (1986); Saunders and Kriebel (1988); Rossow et al. (1989b)]. Cloud amount determined from these results would be overestimated. However, the tests cannot be so strict that the statistics will be insufficiently numerous, biased, or both. No matter how strict the tests are made, some cloud contamination still occurs. In section 4, we present evidence to support the particular numerical values in Table 1.

c. *Cumulation of space/time statistics*

The third ISCCP algorithm step accumulates IR and VIS radiance statistics over various space and time scales. These statistics are used to estimate the clear radiance values by accounting for geographic and time variations of the frequency of occurrence of clear conditions and by providing cross-checks to detect cloud contamination. To obtain a better statistical estimate of clear-sky properties (cf. Rossow et al. 1989b), we seek to increase the number of clear-sky observations over that obtained from a single image. To determine the mode value of the clear-sky radiance distribution, where several observations are possible in a time period that is short compared with the time scale of significant changes in the surface, we attempt to collect observations from several days. To correct those observations mistakenly identified as clear in the first two classification steps, we look for characteristic variations of clear conditions over larger spatial domains or longer time periods (cf. Coakley and Baldwin 1984). To maintain an adequate statistical sample, each 5-day period must contain at least three images at each UTC and each month must have statistics from at least three 5-day periods at each UTC. If too many images are missing for a particular UTC, whole 5-day or month-long periods may have no results.

By comparing these statistics we try to account for the fact that the space–time scales that best separate cloudy and clear radiances vary with location and time of day and year (see section 4). In other words, we must balance between the higher probability of observing clear conditions at larger scales and encountering larger clear variations as the scales increase. Our goal is to choose for each location a space and time domain of observation within which the natural clear-sky variability does not exceed, and perhaps is somewhat smaller than, the chosen radiance threshold in step 5. Thus, the key to this approach is classification of each location by the magnitude of its characteristic space/time variability under clear conditions.

Each image scene is classified by its surface properties into one of the following classes for clear IR radiances (Table 2): 1) open oceans, 2) near-coastal oceans and lakes, 3) polar and other ice-covered water, 4) low and relatively flat land, 5) high and rough topography land, and 6) ice- or snow-covered land. The classifications for clear VIS radiances are (Table 2) 1) open ocean, 2) lakes, 3) open water in polar seas, 4) ice-covered water, 5) densely vegetated land surfaces (forests, woodlands, shrublands), 6) sparsely vegetated (grasslands, tundra), or 7) arid vegetation and unvegetated (desert) land surfaces, 8) polar (snow free) land areas, and 9) ice- or snow-covered land. Each of these classes has an associated "short term" and "long term" time interval for collection of variability statistics (Table 2). The magnitudes of clear radiance variability are also assumed to vary with surface type and to increase with

TABLE 2. Time scales of variability for different surface types.

IR classes	Short term	Long term
Open ocean	15 days	30 days
Near-coastal ocean and lakes	5 days	15 days
Polar seas and ice covered water	5 days	15 days
Land	5 days	15 days
High and rough topography land	5 days	15 days
Ice- or snow-covered land	5 days	15 days
VIS classes	**Short term**	**Long term**
Ocean	—	30 days
Lakes	—	15 days
Polar ocean (open water)	—	15 days
Ice-covered water	5 days	—
Forests, woodlands, shrublands	—	30 days
Grasslands, tundra	—	30 days
Arid vegetation, deserts	—	30 days
Polar land (snow free)	—	15 days
Snow- or ice-covered land	5 days	—

the length of the time interval. For clear IR radiances, the short-term period is selected to approximate the natural time scale for significant variability of the local surface temperature compared with the magnitude of the variability tests applied in the classification steps. The long-term period is selected to encompass variations of more persistent cloud cover. For clear VIS radiances only one time period is needed (cf. Sèze and Rossow 1991a).

For IR we collect time statistics over a small spatial domain, 3×3 scenes, centered on each scene. Statistics collected over the short term (ST) and long term (LT) for each location are the number of observations labeled as clear by the first two algorithm steps ($N_{\text{CLEAR-ST}}$ and $N_{\text{CLEAR-LT}}$), the average IR radiance for these clear scenes ($T_{\text{AVG-ST}}$ and $T_{\text{AVG-LT}}$), and the maximum IR radiance observed without regard to classification ($T_{\text{MAX-ST}}$ and $T_{\text{MAX-LT}}$). In addition the mode of the distribution of differences between two 15-day values of T_{MAX} for each 10° latitude zone (land and water separately) is determined to correct for seasonal trends in surface temperatures. For VIS we collect only the minimum reflectance values ($R_{\text{MIN-ST}}$ or $R_{\text{MIN-LT}}$ as specified in Table 2).

d. Construction of clear-sky composites

Estimates of the clear-sky IR and VIS radiances are made in the fourth ISCCP algorithm step. The goal is to obtain values for each location once every 5 days. Since the values obtained at each location can come from a range of time (and space) scales, we refer to the resulting map, which resembles an image, as a composite.

1) IR CLEAR-SKY COMPOSITE

We require a means to decide for each location and 5-day period whether the location is clear to moderately cloudy or whether the location is highly to persistently cloudy. In the former case, we use the short-term statistics to estimate the clear radiances, whereas in the latter case we use the long-term statistics. In other words, as the amount of cloudiness increases, we are compelled to use progressively less accurate estimates of the clear radiances obtained from observations over larger space–time domains. The tests performed to decide which statistics to use for IR are illustrated in Fig. 2a.

In section 4 we present evidence for the two key statistical tests: 1) whenever the number of clear detections from steps 1 and 2 over any given period is low, it is a reliable indicator of widespread and persistent cloudiness and 2) whenever cloudiness is frequent, it produces broader IR radiance distributions than

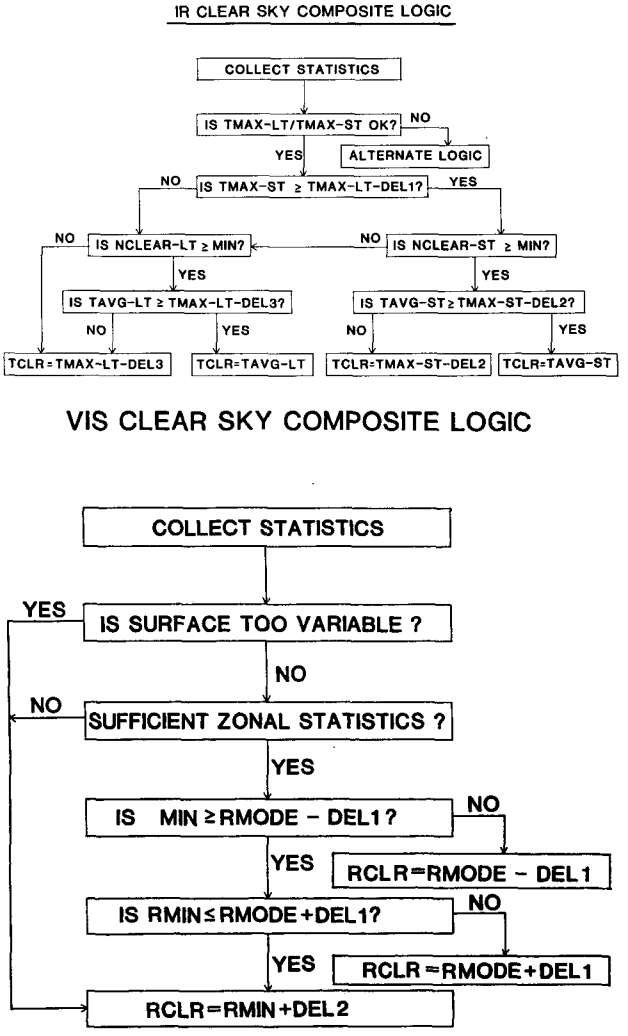

FIG. 2. Logic for determining (a) clear IR radiance values and (b) clear VIS radiance values for each scene at each time. Terms are defined in the text; values of test parameters (e.g., DEL1) are given in Table 3. All comparisons are performed separately for each diurnal phase.

TABLE 3. Test values used in IR and VIS clear-sky composite logic. Infrared values are in kelvins and VIS values in percent scaled radiances.

IR surface types	DEL1	DEL2	DEL3	DEL4
Open ocean	2.0	2.0	2.5	4.0
Near-coastal ocean and lakes	3.0	3.0	4.0	6.0
Polar seas and ice-covered water	3.0	3.0	4.0	6.0
Land	6.0	5.0	8.0	8.0
High or rough topography land	9.0	7.0	11.0	10.0
Ice- or snow-covered land	9.0	7.0	11.0	10.0
VIS surface types				
Ocean	3.0	1.5	—	—
Lakes	3.0	1.5	—	—
Polar ocean (open water)	3.0	1.5	—	—
Ice-covered water	—	5.0	—	—
Forests, woodlands, shrublands	6.0	3.5	—	—
Grasslands, tundra	—	3.5	—	—
Arid vegetation, deserts	—	3.5	—	—
Polar land (snow free)	—	3.5	—	—
Snow- or ice-covered land	—	5.0	—	—

TABLE 4. Cloud detection radiance thresholds used for different surface types. Infrared thresholds are given in kelvins and VIS thresholds are given in percent scaled radiances.

	IR threshold	VIS threshold
Open ocean	2.5	3.0
Near-coastal ocean, lakes	4.0	3.0
Ice-covered water	4.0	12.0
Land	6.0	6.0
High or rough topography	8.0	6.0
Snow-covered land	6.0	12.0

mostly clear conditions (Sèze and Rossow 1991a). In section 4 we show that these two effects are also strongly correlated.

The IR clear-sky composite logic assumes that there is a characteristic shape of the warmer part of the IR radiance distribution that is a function of surface type (section 4, Sèze and Rossow 1991a). The composite logic tests the shape of the distribution of IR radiances by the differences in the values of $T_{\text{AVG-ST}}$, $T_{\text{AVG-LT}}$, $T_{\text{MAX-ST}}$, and $T_{\text{MAX-LT}}$. If differences among these quantities exceed their specified magnitudes (see Table 3), this is interpreted to indicate cloud contamination of the shorter-term statistics. An additional use of this shape assumption is to estimate the value of T_{AVG} for the actual clear IR radiance distribution from T_{MAX} by subtracting a specified amount.

Five situations arise when comparing the magnitudes of cloud-clear radiance contrast and cloudy radiance variability with the variability of the surface. 1) The scene is either partially covered by very low-level clouds that differ little in temperature from clear conditions or completely covered by clouds that are so uniform (in space and time) that they appear statistically similar to clear conditions. This situation is evidenced by narrow IR radiance distributions indicating little space or time variability. 2) The scene is either mostly cloudy with a cloud-clear contrast that is only slightly larger than the clear variability or the cloudiness is very persistent or extensive, but not completely overcast at all times. 3) The scene is mostly cloudy but the cloudy radiances exhibit large space or time variability. 4) The scene is partially cloudy or totally cloudy only occasionally and the cloud-clear contrast is large. 5) The scene is relatively clear.

The first and last cases resemble each other in that the magnitude of the cloudy radiance variations in case 1 is similar to the variations of the surface in case 5 or the cloud cover is complete over the region for 30 days with little variation of cloudy radiances. If the scene is actually clear, then $T_{\text{AVG-ST}}$ will accurately represent clear radiances. If the scene is actually cloudy, but the radiances do not vary very much, the clouds cannot be detected. Two alternative schemes to improve detection in the latter case have been tried with little success: use of comparisons between widely separated regions (large spatial scales > 1000 km) to detect the presence of clouds (cf. Coakley and Baldwin 1984) and use of conventional surface observations of temperature to determine clear IR radiances (cf. Stowe et al. 1988). Neither of these schemes provided sufficient improvement in the accuracy of clear radiance values

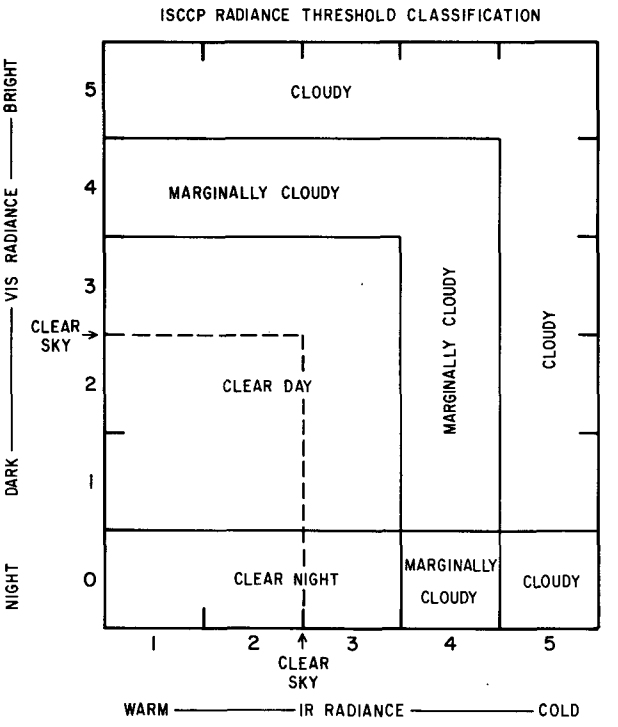

FIG. 3. Schematic of radiance classification of each scene by the radiance threshold tests. Each interval along the axes is equal to the radiance thresholds (Table 4), except for open intervals 1 and 5. VIS class = 0 indicates nighttime.

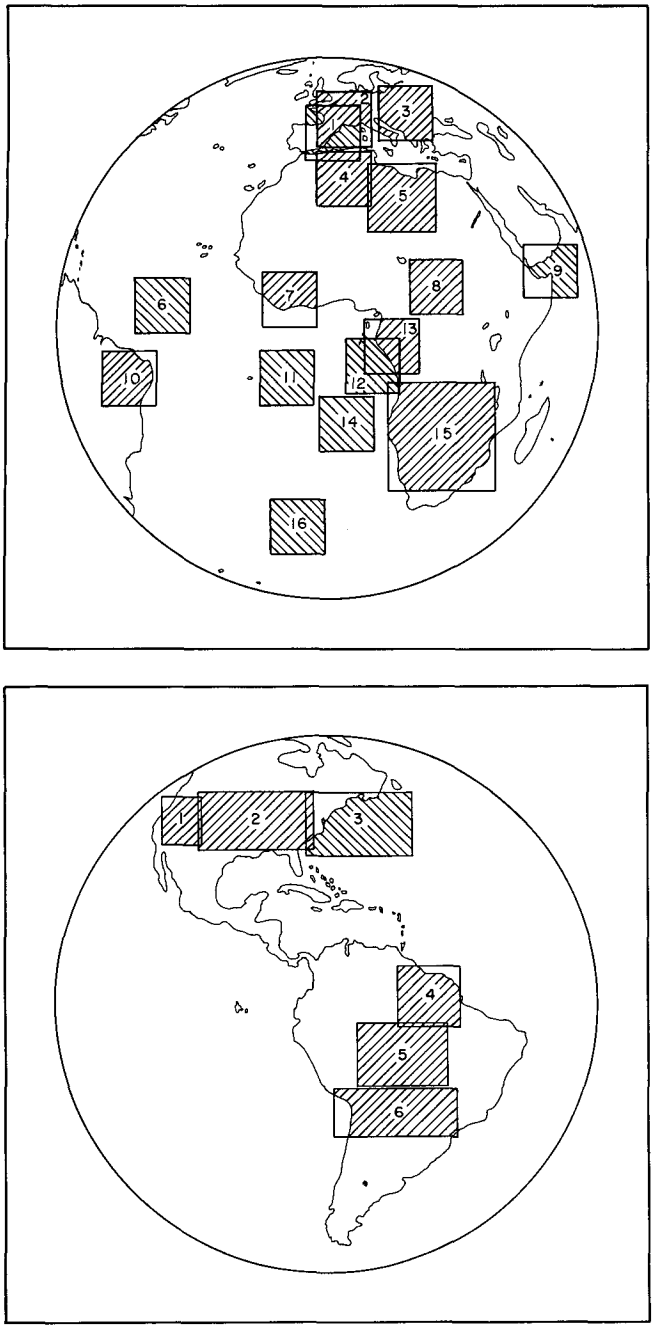

FIG. 4. Special study regions in the view of (a) Meteosat and (b) GOES-East. Regions with hatching slanting to the upper right include scenes from the land areas only, while regions with opposite hatching include water areas only.

to detect the most difficult examples of such clouds (see section 4). The first and last cases (see Table 3) are indicated by $T_{\text{MAX-ST}} \geq (T_{\text{MAX-LT}} - \text{DEL1})$, $N_{\text{CLEAR-ST}} \geq \text{MIN}$, and $T_{\text{AVG-ST}} \geq (T_{\text{MAX-ST}} - \text{DEL2})$, so that $T_{\text{CLR}} = T_{\text{AVG-ST}}$.

The remaining cases depend on whether or not conditions are nearly overcast all the time and on the magnitude of the contrast between clear and cloudy radiances. In case 2, either the radiance variations caused by clouds are relatively small or almost no clear observations are available. This situation is usually revealed by $T_{\text{MAX-ST}} < (T_{\text{MAX-LT}} - \text{DEL1})$ and $T_{\text{AVG-LT}} < (T_{\text{MAX-LT}} - \text{DEL3})$, in which case $T_{\text{CLR}} = (T_{\text{MAX-LT}} - \text{DEL3})$. The value of $T_{\text{MAX-LT}}$ is corrected for any seasonal trends for the particular 5-day period. This test is more useful over oceans, where clear radiances are nearly constant but may be very rare; however, the larger variability of land temperatures makes this test less useful, since DEL1 must be large enough to avoid spurious detections.

In case 3, the cloud–clear radiance contrast is sufficiently large compared to the variability of the surface that the space/time contrast tests correctly detect all of the clouds. However, since the scene is mostly cloudy, too few clear observations are found to estimate the clear radiances reliably. This is indicated by a value of $N_{\text{CLEAR}} < \text{MIN}$, MIN = 3. If the condition occurs only on the short term, then usually $T_{\text{CLR}} = T_{\text{AVG-LT}}$; if the condition occurs on the long term as well, then $T_{\text{CLR}} = (T_{\text{MAX-LT}} - \text{DEL3})$. For both cases 2 and 3, when long-term information is used for T_{CLR}, consistency is maintained by requiring that $T_{\text{CLR}} \geq (T_{\text{MAX-ST}} - \text{DEL2})$.

In case 4, while there are enough clear values available on the short term, there is still too much cloud contamination of $T_{\text{AVG-ST}}$. This is indicated by $T_{\text{AVG-ST}} < (T_{\text{MAX-ST}} - \text{DEL2})$ [a similar condition may occur on the long term as evidenced by $T_{\text{AVG-LT}} < (T_{\text{MAX-LT}} - \text{DEL3})$]. In this case $T_{\text{CLR}} = (T_{\text{MAX-ST}} - \text{DEL2})$ (or $T_{\text{CLR}} = T_{\text{MAX-LT}} - \text{DEL3}$).

Since the composite tests rely on relationships involving $T_{\text{MAX-LT}}$ and $T_{\text{MAX-ST}}$, some protection is required to avoid false results caused by spuriously large IR radiance values occasionally produced by telemetry or data processing errors. This protection is provided by comparing the value of $T_{\text{MAX-LT}}$ for each scene against a regional distribution of $T_{\text{MAX-LT}}$ values: if the particular value is both larger than the tenth-percentile value in the regional distribution by more than DEL4 and larger than its associated $T_{\text{AVG-LT}}$ value by more than DEL4, then it is replaced by the tenth percentile value from the regional distribution ("alternate logic" in Fig. 2a). Any value of $T_{\text{MAX-ST}}$ that is too close (within DEL1) to a replaced $T_{\text{MAX-LT}}$ value is not used in the clear-sky logic.

A final spatial test is applied to ocean regions about 250 km in size to smooth out the effects of radiometer noise over the oceans and to reduce the effects of any remaining spuriously large values. If any region is found to have a range of T_{CLR} values such that [maximum (T_{CLR}) − minimum (T_{CLR})] > DEL3, then all values above the midpoint of the range are replaced by the midpoint value.

One important attribute of the IR compositing process is that the most extreme value of T_{CLR} that can

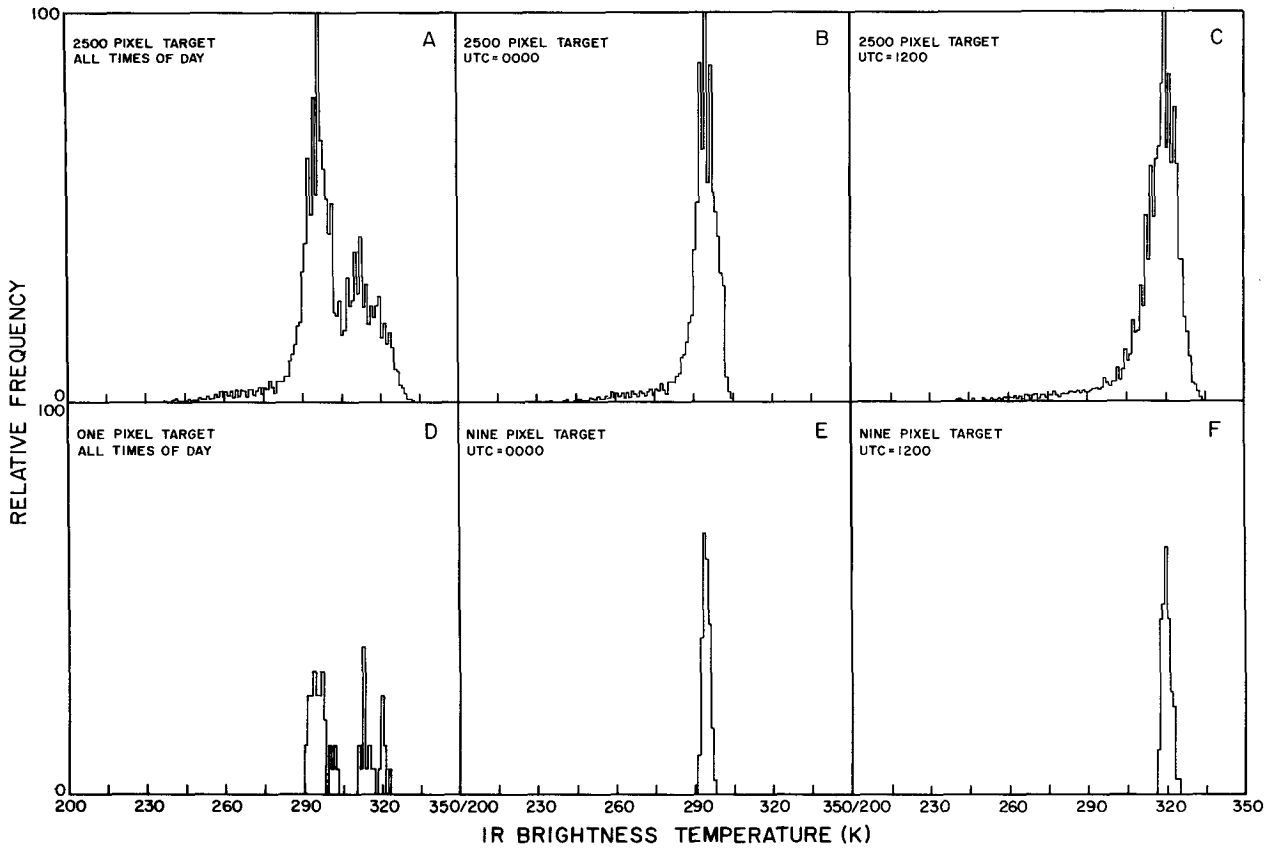

FIG. 5. Frequency distributions of IR radiance values (brightness temperatures in kelvins) for Meteosat region 5 (see Fig. 4a) collected (a) over the whole target at all times of day, (b) over the whole target at 0000 UTC (about one hour after local midnight), (c) over the whole target at 1200 UTC (about one hour after local noon), (d) for one scene (area about 625 km^2) over all times of day, (e) for a nine-pixel target (area about 50, 625 km^2) at 0000 UTC, and (f) for a nine-pixel target at 1200 UTC. All frequencies are normalized, except the lower panels are relative to the frequency for a nine-pixel target over all times of day.

be obtained is $T_{\text{MAX-LT}}$ − DEL3. This ensures that the cloud detection algorithm cannot produce a clear radiance value that is outside the observed long-term distribution of actual values; however, it also means that the clear IR radiance may be cloud contaminated and the cloud amount slightly underestimated in areas with complete and persistent (month long) overcast.

2) VIS CLEAR-SKY COMPOSITE

The procedure used to estimate the clear VIS reflectances (R_{CLR}) is illustrated in Fig. 2b. Unlike the IR, the variations of the VIS clear reflectances are usually smaller in time than space, especially over land; consequently radiance statistics are collected for single scenes. The generally small variations of surface VIS reflectances and their tendency to be smaller than cloud reflectances produce a characteristic shape of the darker part of the VIS radiance distribution that depends only weakly on surface type (section 4, Sèze and Rossow 1991a). The relatively simple behavior of VIS radiances (cf. Reynolds and Vonder Haar 1977) allows use of a simple statistic, the minimum value, to estimate clear values; however, direct use of the minimum introduces some bias (Matthews and Rossow 1987; Rossow et al. 1989a). As we show in section 4, a characteristic correction to the minimum value can be inferred from the shape of the VIS reflectance distribution associated with different surface types.

The surface is classified into nine types, depending on the time scale of VIS reflectance variation and its magnitude (Tables 2 and 3). The clear reflectances for the most rapidly varying land and ocean regions (ice and snow covered) are estimated using a short-term determination of R_{MIN} and a larger correction value: $R_{\text{CLR}} = (R_{\text{MIN-ST}} + \text{DEL2})$.

The remaining types of land have R_{CLR} values that do not vary very much in time, but differ in the magnitude of their spatial variability. The more arid climate regimes are sparsely vegetated and generally exhibit more spatial variability (cf. Matthews and Rossow 1987), but are generally less cloudy; thus, $R_{\text{CLR}} = (R_{\text{MIN-LT}} + \text{DEL2})$ without further adjustment. Vegetated land areas exhibit less small-scale spatial

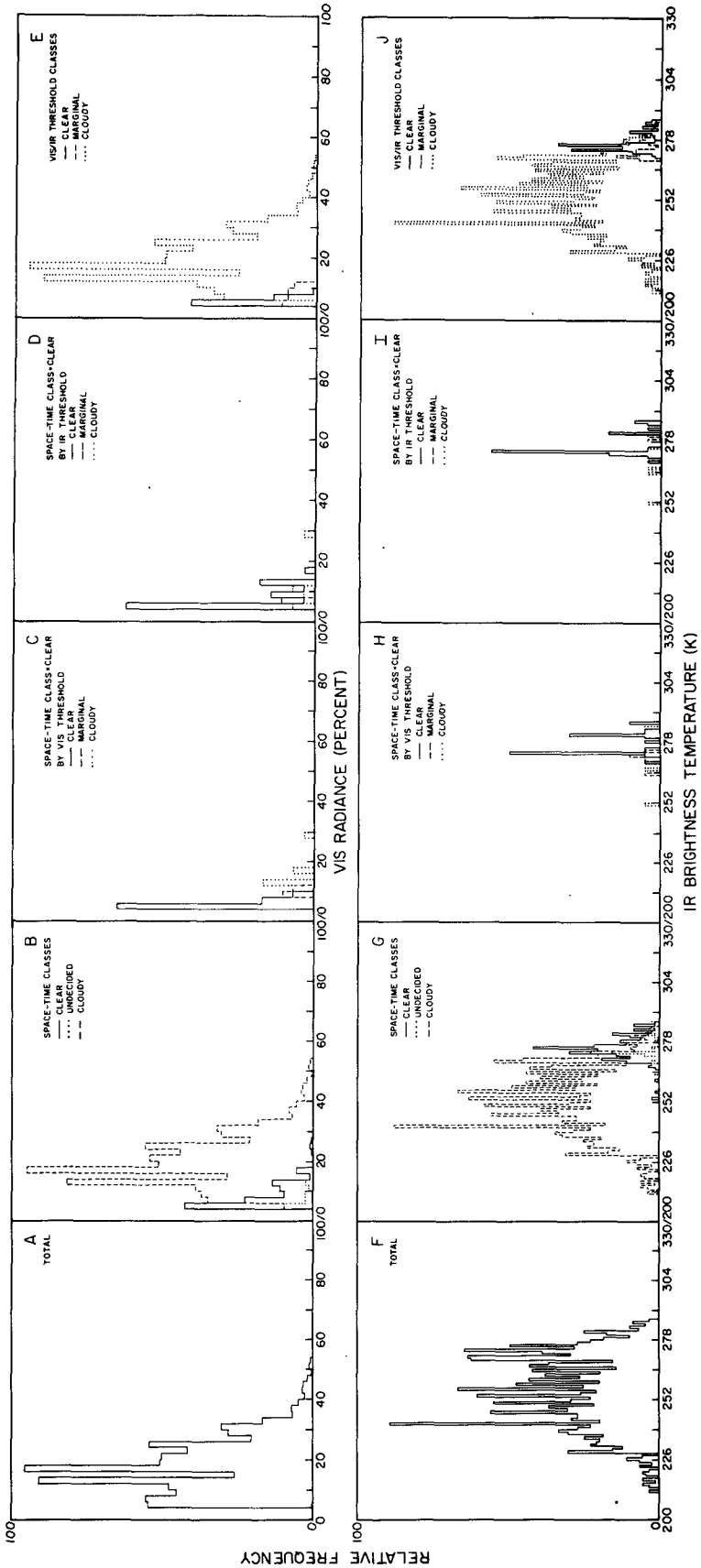

FIG. 6. Frequency distributions of VIS and IR radiances for Meteosat region 16 (see Fig. 4a) for July 1983 at 1200 UTC: (a) total VIS radiance distribution, (b) VIS radiances separated by the space–time contrast tests, (c) VIS radiances classified as clear by the space–time contrast tests and separated by the VIS threshold, (d) VIS radiances classified as clear by the space–time contrast tests and separated by the IR threshold, (e) final separation of VIS radiances by the VIS/IR radiance threshold tests, and (f)–(j) IR radiance distributions corresponding to (a)–(e).

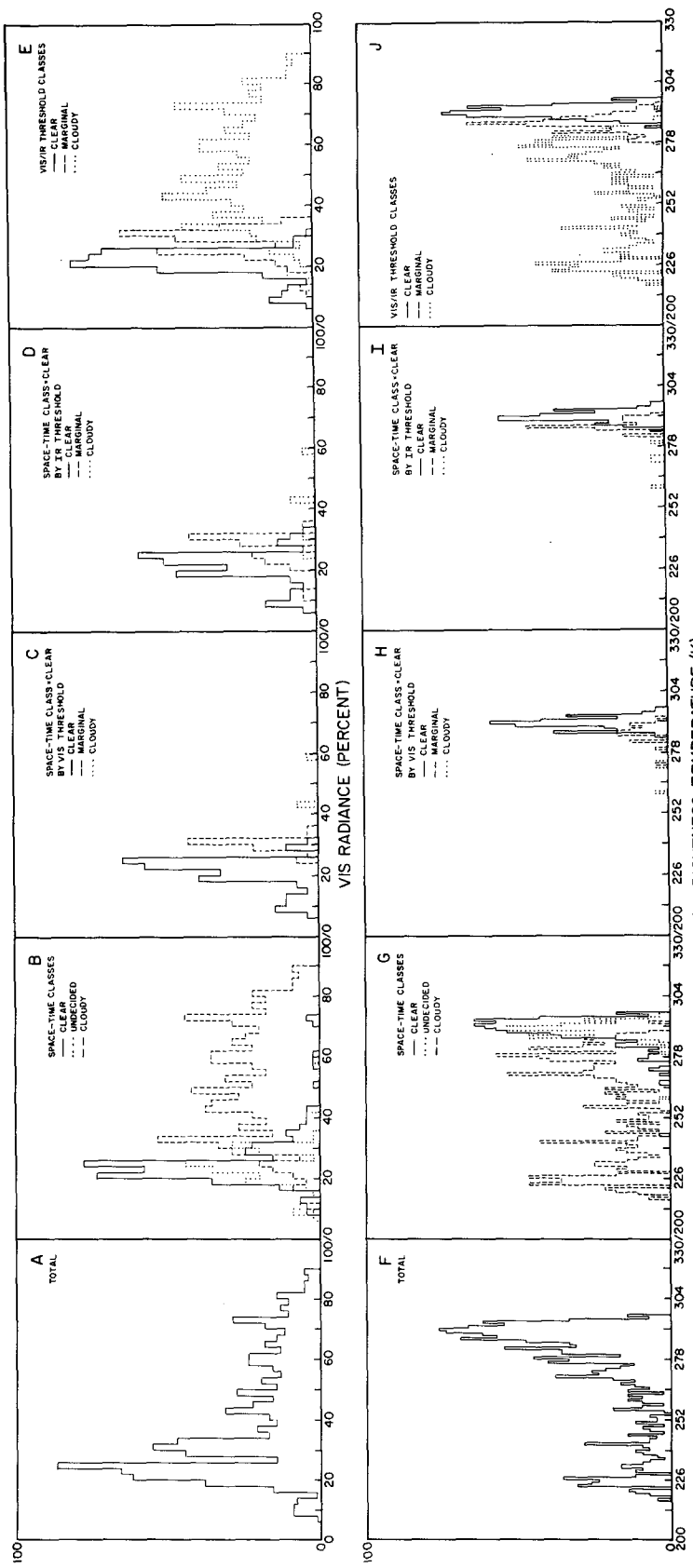

FIG. 7. Same as Fig. 6 for Meteosat region 3.

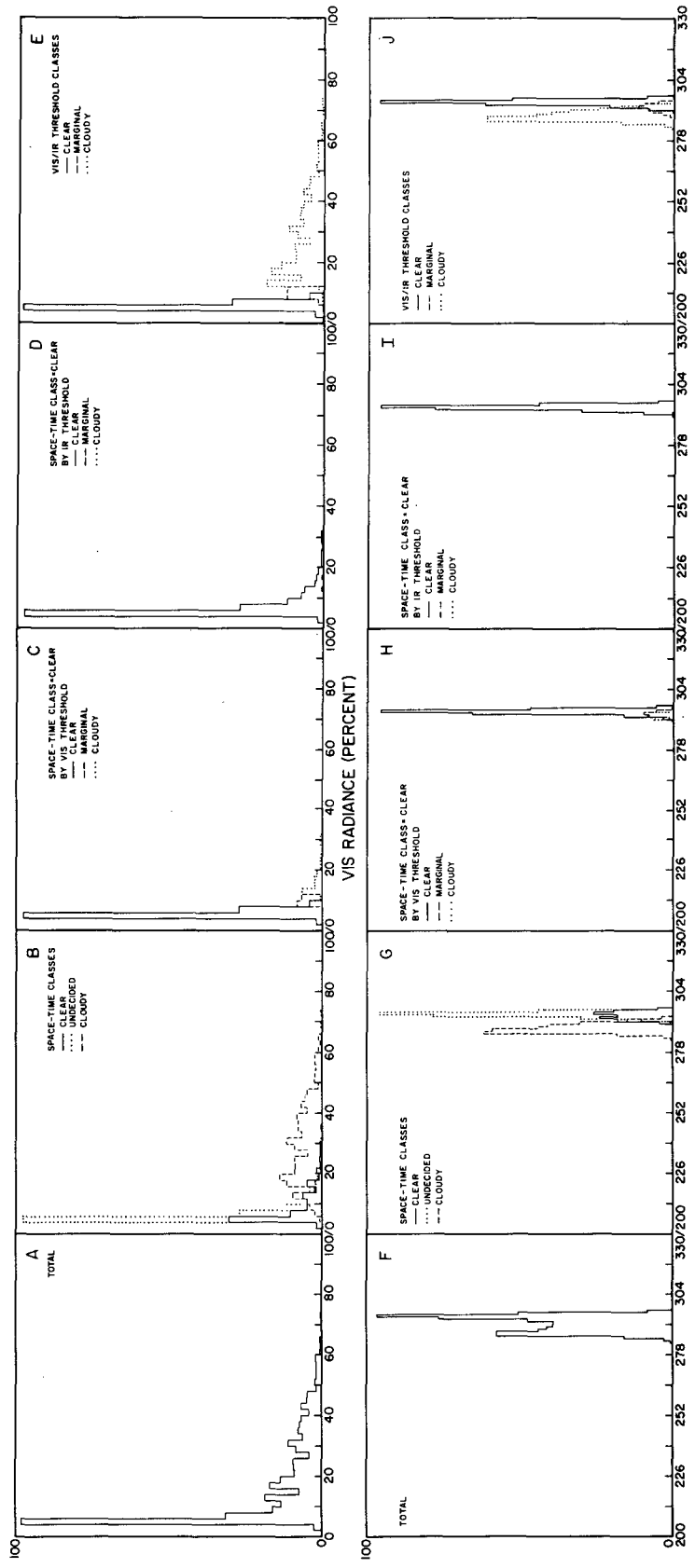

FIG. 8. Same as Fig. 6 for Meteosat region 11.

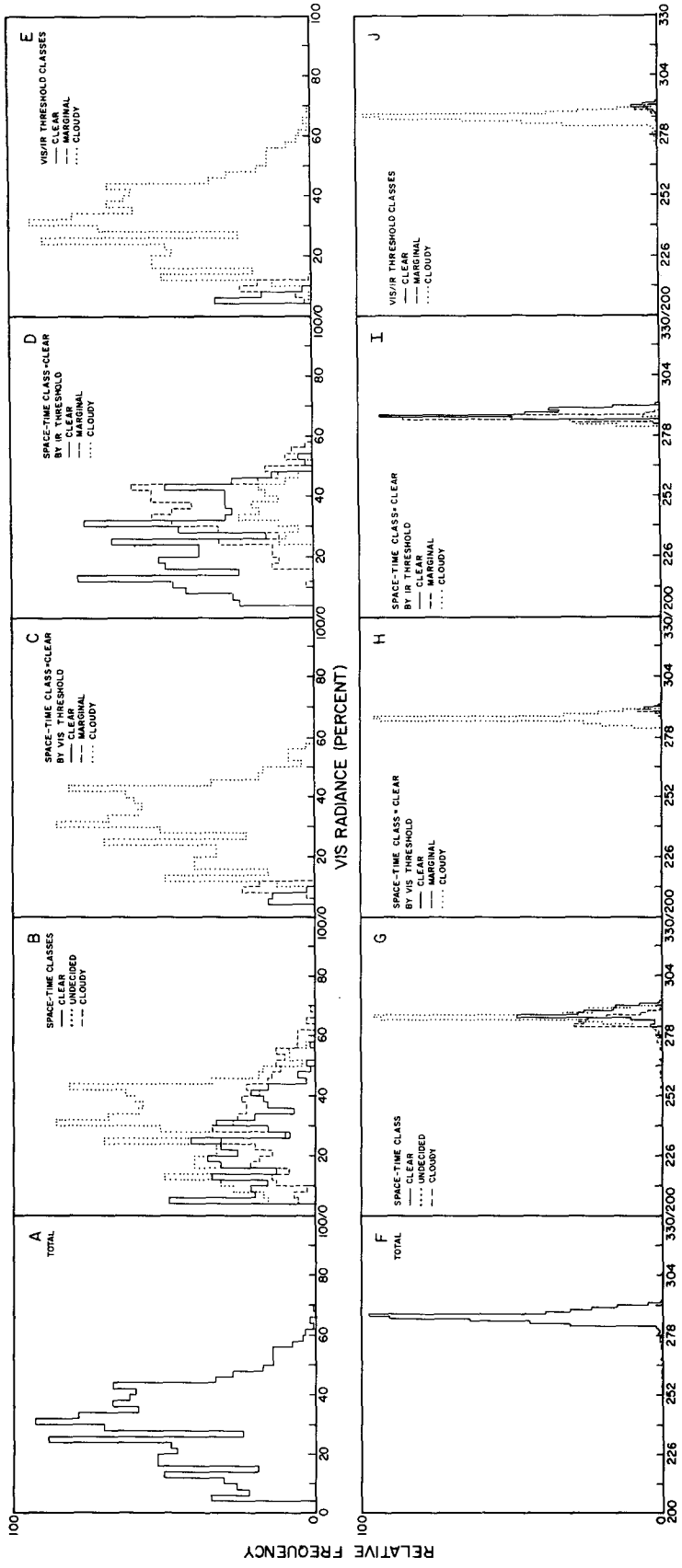

FIG. 9. Same as Fig. 6 for Meteosat region 14.

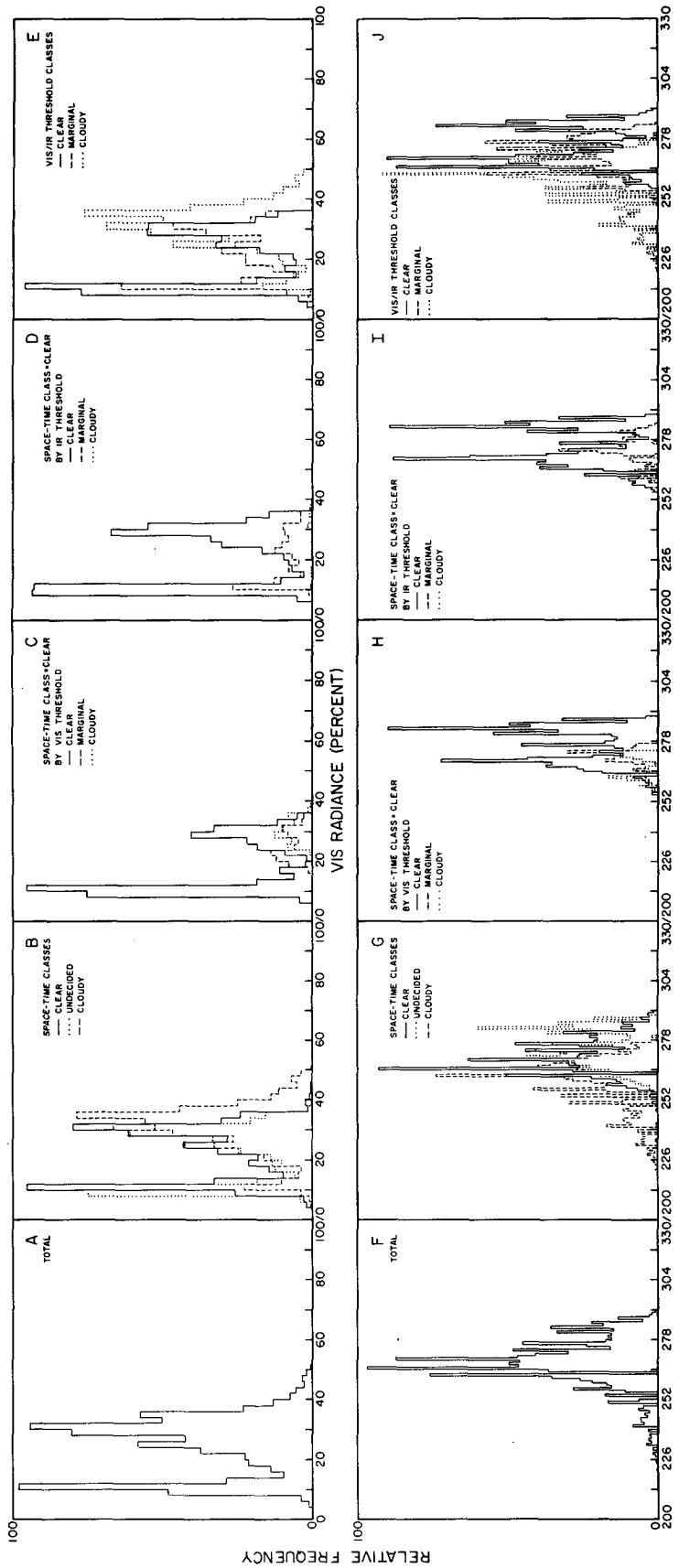

FIG. 10. Same as Fig. 6 for GOES-East region 2 for January 1984 at 1800 UTC (see Fig. 4b).

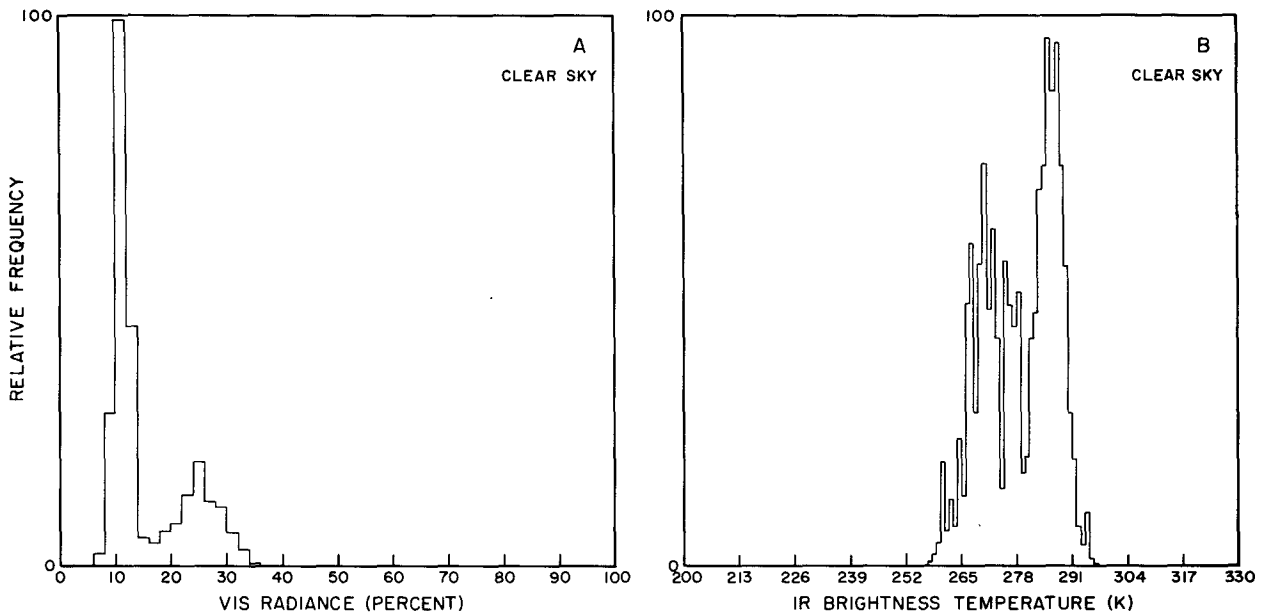

FIG. 11. Frequency distribution of clear VIS and IR radiances for GOES-East region 2 for January 1984 at 1800 UTC, corresponding to the analysis illustrated in Fig. 10.

variability and are more uniform from one geographic location to another. Hence after calculating $R_{CLR} = (R_{MIN\text{-}LT} + DEL2)$, individual values within each latitude zone are compared to the distribution of all R_{CLR} values for the same vegetation cover types and are required to be within ±DEL1 of the distribution

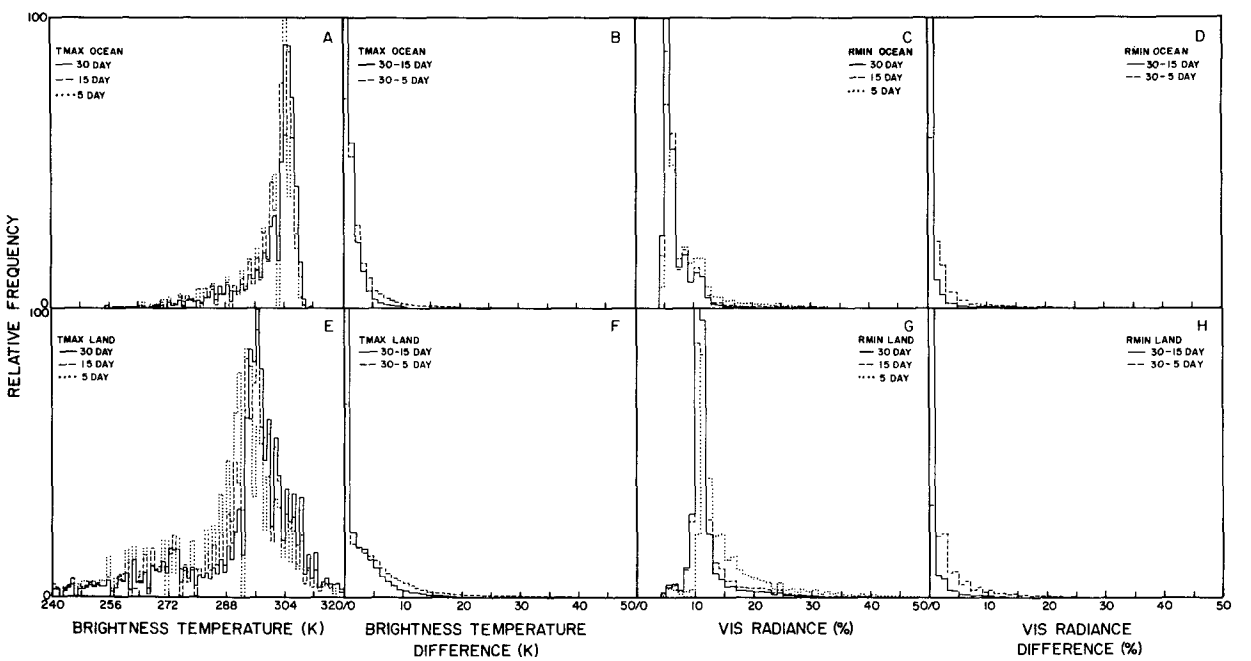

FIG. 12. VIS/IR radiance statistics from the whole GOES-East region (Fig. 4b) for January 1984: (a) maximum IR radiances (brightness temperature) for each ocean scene collected over a 5-day period (dotted line), a 15-day period (dashed line), and a 30-day period (solid line), (b) differences between 5-day and 30-day T_{MAX} values (dashed) and between 15-day and 30-day T_{MAX} values (solid) for each ocean scene, (c) minimum VIS radiances (reflectances) for each ocean scene collected over 5-, 15-, and 30-day periods, (d) differences between 5- and 30-day and between 15- and 30-day R_{MIN} values for each ocean scene, and (e)–(h) corresponding distributions for land scenes.

TABLE 5. Changes in clear-sky composite IR radiances, associated values of clear VIS radiances, and cloud amount caused by decreasing the DEL1, DEL2, and DEL3 values by a factor of two. The IR clear fraction (in percent) is the fraction of daytime clear scenes determined to be clear using the IR threshold only; the associated average value of R (in percent) is shown as R_{CLR} (IR-only). The difference between results with one-half the standard values and the results with the standard values are shown. Values in parentheses give the standard results. The standard value of T_{CLR} is given in kelvins and cloud amount and R_{CLR} are in percent. Regions are indicated in Fig. 4a.

Meteosat region number	T_{CLR}	R_{CLR}	IR clear fraction	R_{CLR} (IR-only)	Cloud amount
1 Mediterranean	0.7 (292.8)	0.0 (6.3)	−3 (73)	−0.1 (6.5)	0.9 (54.6)
2 W. Europe	0.1 (296.6)	0.0 (22.9)	−4 (68)	−0.5 (22.8)	0.7 (55.0)
3 E. Europe	0.2 (291.0)	0.0 (22.2)	−1 (30)	−0.1 (24.3)	0.0 (90.0)
4 Northwest Africa	0.4 (321.8)	0.0 (35.1)	−1 (78)	0.1 (34.3)	0.5 (35.3)
5 Libya	0.3 (320.0)	0.0 (37.0)	0 (95)	0.0 (36.3)	0.1 (30.7)
6 ITCZ-water	0.1 (292.9)	0.0 (5.6)	0 (46)	0.0 (7.4)	0.0 (86.3)
7 Guinea	0.0 (291.7)	0.0 (23.0)	0 (100)	0.0 (35.3)	0.0 (77.6)
8 ITCZ-land	0.2 (298.0)	0.0 (21.0)	−1 (20)	−0.1 (22.1)	0.5 (88.5)
9 Red Sea	0.0 (292.8)	0.0 (9.8)	0 (59)	0.0 (10.7)	0.3 (92.1)
10 Brazil	0.0 (291.8)	0.0 (14.0)	0 (93)	0.0 (15.6)	0.0 (48.8)
11 Trade cumulus	0.0 (293.2)	0.0 (5.4)	0 (56)	0.0 (7.5)	0.0 (73.2)
12 Atlantic coast	0.1 (292.9)	0.0 (18.1)	0 (88)	0.0 (29.5)	0.0 (75.6)
13 Congo	0.0 (290.9)	0.0 (18.1)	0 (99)	0.0 (31.4)	0.0 (71.0)
14 Stratus	0.2 (289.1)	0.0 (5.7)	−1 (40)	0.0 (22.4)	0.0 (99.3)
15 S. Africa	0.6 (302.7)	0.0 (16.0)	−2 (67)	0.0 (16.3)	0.5 (60.0)
16 S. Atlantic	0.1 (280.6)	0.0 (5.2)	0 (11)	0.0 (7.3)	0.1 (94.6)

mode value, R_{MODE}. If a particular value of R_{CLR} violates this condition, it is replaced by $R_{MODE} \pm$ DEL1, whichever is closer in value.

The reflectance of open water is strongly dependent on illumination/viewing geometry; in certain geometries the glint reflectance can be very large and very sensitive to the roughening effect of surface winds. Thus, although we calculate $R_{CLR} = (R_{MIN\text{-}LT} + DEL2)$ for water surfaces, this value is not allowed to be brighter than values predicted from a reflectance model by more than DEL1 nor darker than these values. This reflectance model is a refinement of the model developed by Minnis and Harrison (1984) with the results extended to a larger range of geometries with a representation of glint reflectances that has larger peak values.

3) CLEAR RADIANCES

Estimates of T_{CLR} and R_{CLR} for each scene, once every 5 days, are assembled into the clear-sky composites. Inverse corrections for satellite viewing geometry variations are then applied to simulate the angle dependence of clear radiances for each individual image scene. We call these clear radiances ICLR and VCLR. We show in section 4 and in a companion paper (Rossow and Garder 1993) that the space/time variations of these clear radiances represent the actual variations of surface properties to good accuracy.

e. Radiance thresholds

The final step of the cloud detection is a comparison of each observed radiance value against its corresponding clear-sky composite value [Eq. (3)]. This final classification of the image scenes into cloudy and clear categories is done without regard to any previous classification (although statistics on conflicts are kept to monitor the quality of the analysis). Note particularly that this step does not use VIS reflectances, rather it uses VIS radiances:

$$\begin{aligned} \text{clear:}\quad & (\text{ICLR} - \text{IR}) \leq \text{IRTHR} \quad \text{and} \\ & (\text{VIS} - \text{VCLR}) \leq \text{VISTHR} \\ \text{cloudy:}\quad & \text{ICLR} - \text{IR}) > \text{IRTHR} \quad \text{or} \\ & (\text{VIS} - \text{VCLR}) > \text{VISTHR} \end{aligned} \tag{3}$$

where the values of IRTHR and VISTHR are given in Table 4. At night when there is no VIS, only the IR conditions in (3) are used. During daytime, application of both conditions in (3) is referred to as the VIS/IR result; the results from the first conditions, called the IR result, are also reported during daytime. Each image scene is classified in more detail by the relative position of its radiances, IR and VIS, with respect to ICLR and VCLR (Fig. 3). In particular, marginally cloudy scenes (a subset of cloudy) are identified as scenes with radiances that differ from the clear values by more than the threshold amount, but by less than twice the threshold amount.

There are three specific exceptions to (3) applied in particular situations. Because of the large and unpredictable variations of ocean VCLR in glint geometry and near snow and sea ice margins, the VIS data are not used for detections of clouds in these locations. Because of the larger uncertainty in VCLR over snow and sea ice, the magnitude of the VIS threshold is doubled to 12%. Because occasional errors in the earth location information can shift the position of the

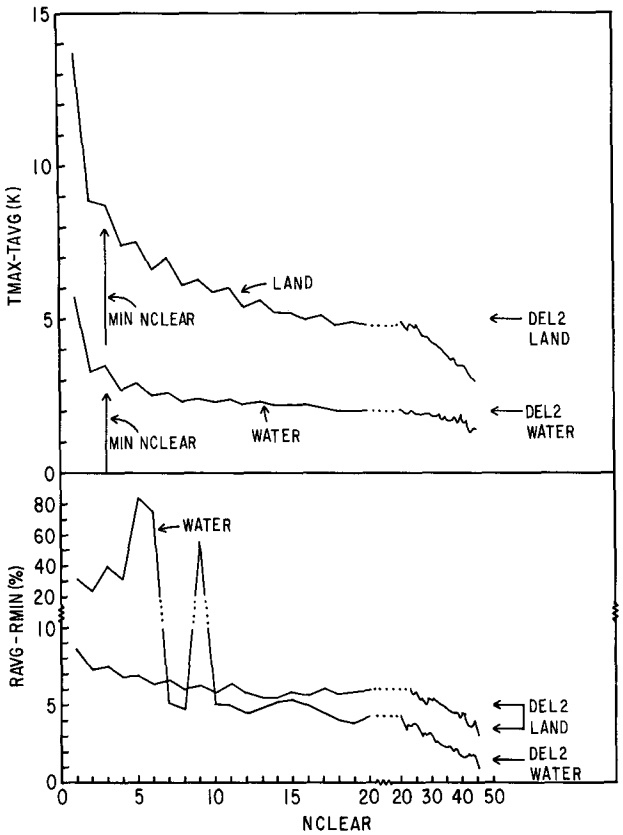

FIG. 13. Average values of T_{MAX} minus T_{AVG} (upper panel) from Fig. 12b and 12f and R_{AVG} minus R_{MIN} (lower panel) from Fig. 12d and 12h sorted by the value of N_{CLEAR} for land and water areas (see text for definitions). The minimum of N_{CLEAR} used in the clear-sky compositing step is indicated by a solid arrow; the dashed arrow indicates an alternative value used to test the sensitivity of the cloud detection. The value of DEL2 (cf. Fig. 2a and Table 3) is used to compare T_{MAX} and T_{AVG} in the clear-sky compositing step. Results are a combination from the Meteosat and GOES-East regions for July 1983 and January 1984.

coastlines in a particular image relative to its assumed position, the daytime contrast in ICLR and VCLR between the land and ocean can produce spurious cloud detections. This is inhibited by requiring confirmation of marginal IR detections (see Fig. 3) near the coast by the VIS channel in daytime conditions.

Since the clear radiances are estimates, their values are uncertain. Clouds are identified to be present only when they alter the observed radiances by more than the uncertainty in the clear radiance values. The magnitudes of the uncertainties in ICLR and VCLR depend on the surface type (Table 4). In other words, the threshold for cloud detection is the estimated magnitude of the uncertainty in the clear radiance estimates. Note that many authors refer to the clear radiance value itself as the threshold. The ISCCP method can be described as a "constant threshold" method only when "threshold" refers to the difference between the clear and observed radiances.

4. Supporting statistics and sensitivity test results

In this section we illustrate the situation dependence of the algorithm tests and show evidence supporting the choices of particular test parameter values. Sèze and Rossow (1991a) identified several types of radiance behavior by the shapes of the radiance histograms. Guided by these results, we select several specific regions (Fig. 4) to illustrate the detailed behavior of the cloud detection algorithm and to demonstrate the performance of the algorithm in some particularly difficult situations. Finally, we estimate the uncertainty in the cloud detection from the sensitivity of the results to small changes in test parameter values.

a. Radiance variations

We reduce the magnitude of time variations of clear radiances by analyzing the data at constant diurnal phase. Using a nearly cloud-free desert (region 5 in Fig. 4a) as an extreme example of diurnal temperature variability, we contrast the diurnal and day-to-day variations of surface temperature with their spatial variability in Fig. 5. The distribution of T (IR brightness temperatures) over the whole area for one week at all times of day is quite broad, including the effects of infrequent cirrus clouds (Fig. 5a). Even when individual scenes are considered, the dispersion is nearly as large (Fig. 5d). That the major source of this dispersion is the diurnal variation of surface temperature is shown by the much narrower distribution found when observations are collected over the whole week but only at

TABLE 6. Relative populations of scenes classified using short-term and long-term statistics and the effect of changing the minimum N_{CLEAR} from 2 to 9. Number of scenes is shown as percentage of total, T_{CLR} is given in kelvins, and cloud amount (CA) is given in percent.

	# − ST	# − LT	T_{CLR}	IR-only CA	CA
Ocean					
minimum N_{CLEAR} = 2	85.9	14.1	284.7	58.8	67.6
minimum N_{CLEAR} = 9	66.9	33.1	284.5	56.9	67.1
Land					
minimum N_{CLEAR} = 2	82.6	17.4	302.2	33.9	41.6
minimum N_{CLEAR} = 9	57.6	42.4	302.1	33.6	41.4

TABLE 7. Effect on cloud amount of substituting T_{max} from 5-, 15-, and 30-day periods in place of T_{CLR} in IR threshold test. All quantities are shown as percent of total number of scenes.

Surface type	T_{MAX} period	Fraction changed CLR to CLD	Fraction new clouds		Fraction changed CLD to CLR	Net change cld amt
			CLR by VIS	CLD by VIS		
Ocean	5	4.7	2.7	2.0	9.1	−4.4
	15	10.7	6.9	3.8	1.6	+9.1
	30	15.0	10.0	5.0	0.4	+14.6
Land	5	6.7	5.6	1.1	3.9	−2.8
	15	17.7	14.9	2.8	0.8	+16.9
	30	25.8	21.6	4.2	0.5	+25.3

one time of day (Figs. 5b and 5c). The spatial variations over the whole region produce less variation than that associated with the diurnal cycle (compare Figs. 5b with 5e and 5c, and 5f with 5a and 5b).

A similar result is obtained for R (VIS reflectances), where the largest effect is changing illumination as the sun rises and sets (not shown). When diurnal variations of illumination are removed, the remaining anisotropy effects are about as large as spatial variations. All subsequent discussions of time variations in this paper, unless explicitly noted, assume constant diurnal phase.

Sèze and Rossow (1991a) summarize the general characteristics of VIS/IR radiance distributions collected over both space and time in terms of two different populations: one relatively dark/warm population that does not vary much in space or time (clear scenes or the surface) and one relatively bright/cold population that varies more in space and time (clouds). The clear population is associated with the modal value of the distribution since the atmosphere is nearly transparent at these particular wavelengths, producing little radiance variability, and the surface properties do not vary much. Consequently, the minimum VIS and maximum IR values are usually similar to their respective mode values. Time variations at a point are generally larger than the spatial variations on scales of only a few hundred kilometers (Sèze and Rossow 1991a). If we collect the time distribution of radiances at each image scene and identify its modal value and then look at the distribution in space of these modal values [e.g., Fig. 12c and 12d in Sèze and Rossow (1991a)], we find that the variation is generally very small, except when near a coastline or an area with persistent cloudiness. Likewise, if we collect the spatial distribution of radiances at one time and identify its mode value and then look at the time distribution of these modal values [Fig. 8 in Sèze and Rossow (1991a)], we again find that the variation is small. For the total radiance distribution the range of values encountered generally increases as the size of the time period or spatial domain grows. These results serve as the basis of the ISCCP cloud detection algorithm design.

b. Space/time classification tests

To illustrate the behavior of the IR space/time contrast test results (Fig. 1), we show how the total VIS/IR radiance distributions in some of the test regions are divided into cloudy, undecided, and clear categories (the mixed category is usually very rare and is not shown in the figures). Figures 6–10 show several examples, some where this portion of the algorithm is successful and some where it is not. Since the independent VIS analysis is usually simpler and easier to interpret, we use the VIS distribution and threshold test results to evaluate the IR space/time contrast tests.

Figures 6a and 6f show the radiance histograms for a region of southern midlatitude oceans (region 16 in Fig. 4a) in July 1983, where the cloud amount is very high (over 92%), but the clouds cause relatively large variations in both the VIS and IR radiances (>20% and >30 K, respectively) as illustrated by the broad distribution shapes. Figures 6b and 6g show the VIS and IR radiances separated by the IR space/time contrast tests into clear, undecided, and cloudy categories: 80% of the scenes are classified as cloudy with about 12% clear and about 2% undecided.[2] The very small population of undecided indicates that the radiance variability produced by clouds is large. The VIS radiances show evidence that about 35% of the clear scenes are clouds (VIS radiances > 10%), as illustrated in Fig. 6c, where the VIS threshold is applied to the VIS radiances of the clear scenes[3]; however, Fig. 6h, which shows the IR radiances associated with the clear scenes separated by the VIS threshold, indicates that these few scenes do not bias the regional average clear IR value by very much. Figures 6d and 6i, which show the VIS and IR radiances for the clear scenes separated by the IR threshold, indicate that about 25% of the apparently clear VIS values are actually thin cirrus clouds (detected by the IR threshold but not the VIS threshold) and that the clear-sky composite procedure has removed enough of the contamination to allow the

[2] All fractions mentioned in the following discussion are determined from the numerical versions of the histograms illustrated in Figs. 6–10.

[3] For Figs. 6–10, step 5 of the algorithm is applied to either VIS or IR radiances that have been classified by steps 1 and 2 into categories of clear, undecided, and cloudy. Since steps 1 and 2 are performed on IR radiances, the VIS threshold results provide an independent consistency check.

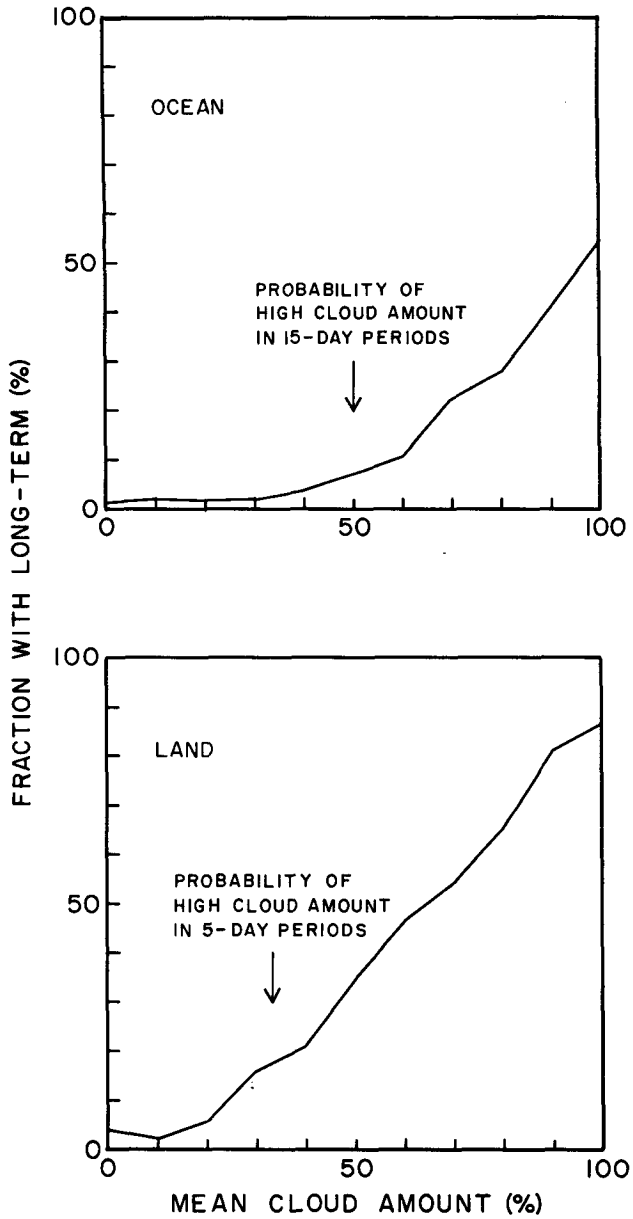

FIG. 14. Fraction of area where clear-sky radiance values come from long-term statistics as a function of the monthly mean cloud amount for ocean (upper panel) and land (lower panel) areas. Results are a combination from the Meteosat and GOES-East regions over July 1983 and January 1984. Arrows indicate the monthly mean cloud amount at which the short-term period used (15 days for ocean, 5 days for land) for clear radiance statistics has a high probability of being completely cloud covered.

IR threshold analysis to detect almost all of the contaminating clouds (discussed in section 4c). Figures 6e and 6j show the final radiance threshold division of the VIS and IR radiances for this region.

Figure 7 shows a similar case over eastern Europe (region 3 in Fig. 4a) with a cloud amount of about 76%, but the more complex radiance distributions also illustrate that the mountainous land background can be more confusing than the oceans (Figs. 7a and 7f). Again the IR space/time contrast tests appear to separate the cloudy (56%) and clear (25%) portions of the radiances well, although there are many more (14%) undecided scenes than for the ocean case (Figs. 7b and 7g), because the algorithm tests assume that larger variations of clear radiances are possible. Figures 7c and 7h show that there is about 25% cloud contamination of the clear scenes, but that this has little effect on the average IR radiances. Figures 7d and 7i show that the clear-sky compositing allows the IR threshold to detect these contaminating clouds. Note in Fig. 7d that there is more thin cirrus in the VIS radiance distribution than over the ocean (as indicated by the IR threshold detections of scenes that have low VIS and relatively high IR radiances—very thin cirrus transmit enough radiation from below to appear relatively warm).

Figure 8 shows a case with moderate, but broken, cloud cover (about 60%) at low levels over the subtropical Atlantic (region 11 in Fig. 4a). Despite the low cloud tops, the IR radiance distribution (Fig. 8f) shows a distinct cloud population, which is more apparent in the VIS distribution (Fig. 8a). In this case, the IR space/time contrast tests successfully separate the cloudy from clear scenes; however, over 35% of the scenes are labeled undecided (Figs. 8b and 8g). Figure 8b shows that most of these undecided scenes have VIS radiances that resemble the clear values. The clear VIS radiances show little (17%) cloud contamination (radiance values > 10%) and little effect on the IR radiances for the clear category (Figs. 8c and 8h), but Figs. 8d and 8i show that this contamination is not removed by the IR threshold. Although such clouds are detected during the daytime by the VIS threshold, they are missed at night. For this case, the underesti-

TABLE 8. Relative population of scenes in each IR space/time category (cloudy, undecided, mixed, and clear) that are classified as cloudy, marginally cloudy, and clear by the VIS/IR threshold test; total shows the percent fraction of the total population classified into each IR space/time category. Each entry shows the ocean value with the land value in parentheses.

VIS/IR threshold class:	Clear	Marginally cloudy	Cloudy	Total
Space/time class for Jul 83 (MET)				
Clear	70 (84)	10 (8)	20 (8)	29 (38)
Undecided	63 (78)	14 (15)	23 (7)	26 (31)
Mixed	5 (25)	9 (27)	86 (48)	7 (4)
Cloudy	2 (4)	6 (17)	92 (79)	38 (27)
for Jan 84 (GOE)				
Clear	87 (70)	8 (17)	5 (13)	24 (13)
Undecided	69 (63)	16 (21)	15 (16)	22 (30)
Mixed	6 (11)	15 (19)	79 (70)	5 (5)
Cloudy	2 (4)	7 (10)	91 (86)	49 (52)

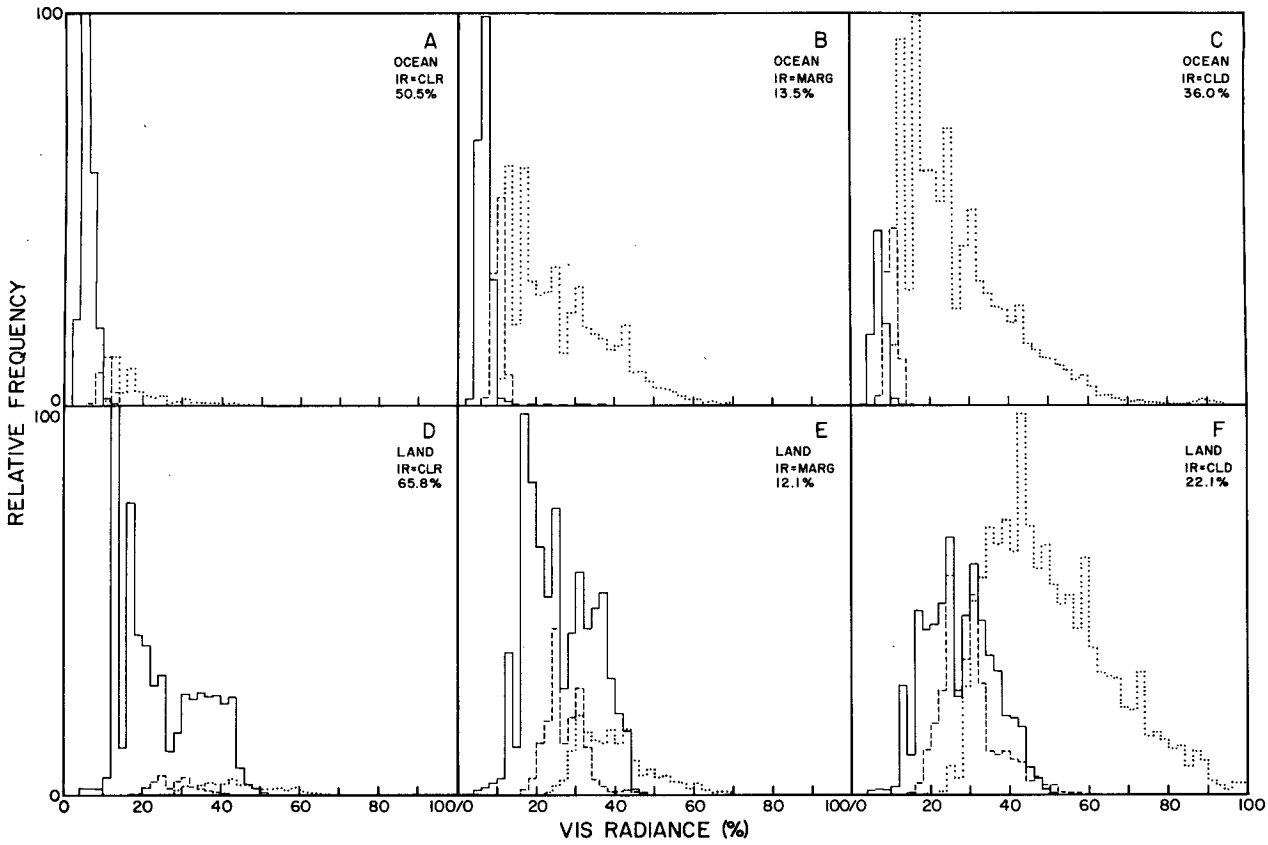
A
OCEAN
IR=CLR
50.5%
B
OCEAN
IR=MARG
13.5%
C
OCEAN
IR=CLD
36.0%
D
LAND
IR=CLR
65.8%
E
LAND
IR=MARG
12.1%
F
LAND
IR=CLD
22.1%
RELATIVE FREQUENCY
VIS RADIANCE (%)

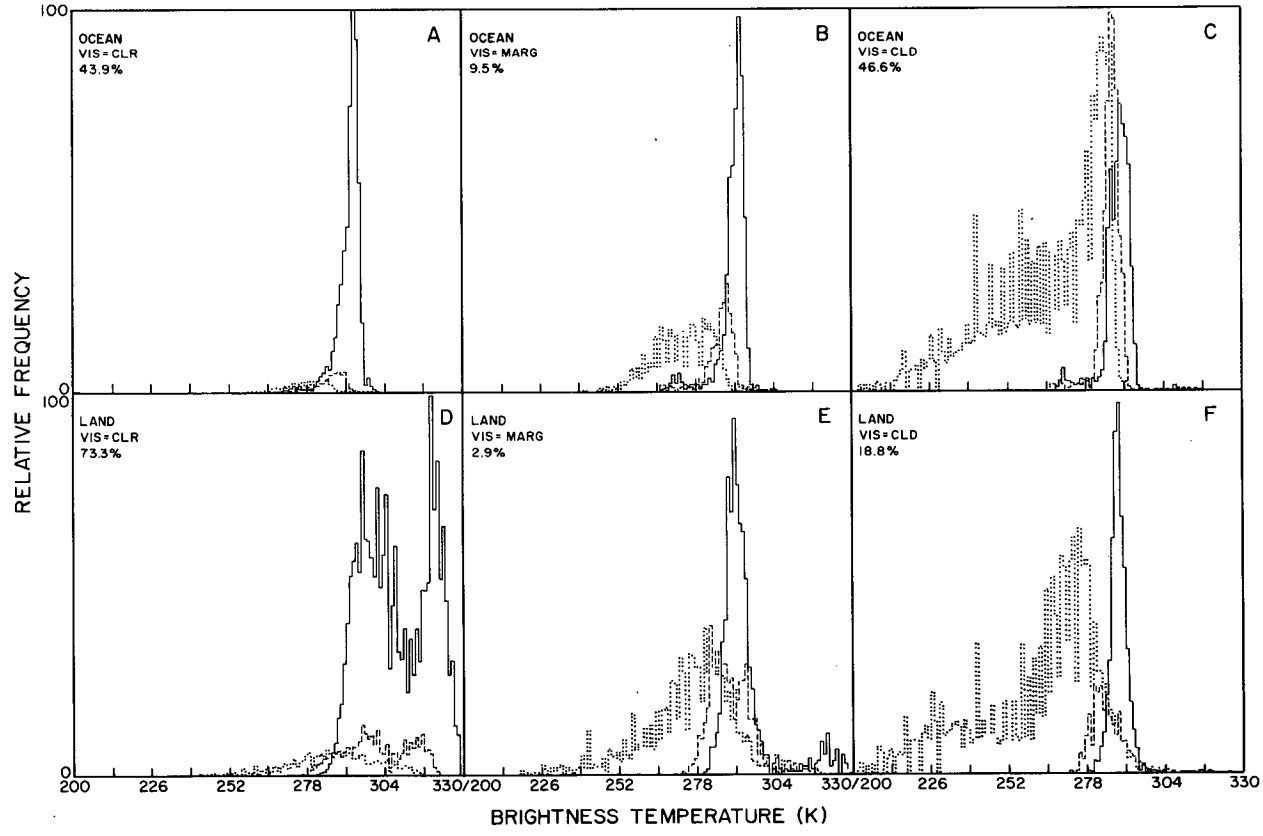
OCEAN
VIS=CLR
43.9%
A
OCEAN
VIS=MARG
9.5%
B
OCEAN
VIS=CLD
46.6%
C
LAND
VIS=CLR
73.3%
D
LAND
VIS=MARG
2.9%
E
LAND
VIS=CLD
18.8%
F
RELATIVE FREQUENCY
BRIGHTNESS TEMPERATURE (K)

mate of the nighttime cloud amount would be about 3%–5%.

Figure 9 shows a much more difficult case of marine stratus clouds in the South Atlantic (region 14 in Fig. 4a). The VIS radiance distribution indicates a larger cloud amount and brighter clouds; however, the IR radiance distribution shows no sign of distinct cloudy and clear populations (Figs. 9a and 9f). Figures 9b and 9g show that the IR space/time contrast tests are only partially successful in separating the cloudy and clear scenes; the "confusion" is indicated by more than 40% of the scenes being labeled undecided and by a much larger population of mixed scenes (almost 20%, not shown). Comparing Figs. 9b and 9g shows that even though much of the brighter cloudiness is labeled undecided, these clouds have slightly larger IR radiance values than the cloudy category. Figure 9c shows that over 90% of the clear scenes are, in fact, clouds; however, Fig. 9h shows that this contamination only shifts the IR radiance value associated with clear conditions by about 5 K. Figures 9d and 9i show that the clear-sky compositing step successfully shifts the clear IR radiance value enough to allow the IR threshold to detect about 45% of the contaminating clouds. However, at night when no VIS test is possible, cloud amount would be underestimated by about 10%–15% as opposed to an underestimate of 25%–30% without the compositing step. Figures 9e and 9j show how difficult this case was: since the actual cloud amount is about 95%, very little clear sky is available to determine the clear radiance values. Even more extreme cases of this type occur in some regions (e.g., region 13 in Fig. 4a—not shown) with complete overcast conditions persisting for the whole month.

Figure 10 shows another difficult case, cloudiness over a partially snow-covered area in central North America (region 2 in Fig. 4b in January 1984). The VIS radiance distribution (Fig. 10a) shows a bimodal structure; there are both snow-covered and snow-free areas present, so the radiances associated with the clouds are not readily apparent (cf. Rossow et al. 1985). The IR radiance distribution (Fig. 10f) shows hints of three populations. The IR space/time contrast tests separate the scenes into three roughly equal groups; the undecided scenes have very similar VIS and IR radiance distributions to the clear scenes, while the cloudy scenes are concentrated at values slightly higher in VIS and generally lower in IR (Figs. 10b and 10g). The VIS threshold division of the clear scenes, if it is trustworthy, indicates only a small amount (about 25%) of cloud contamination that changes the average IR radiance value only a little (Figs. 10c and 10h). The IR threshold separation of the clear scenes (Figs. 10d and 10i) indicates the presence of significant amounts of thin cirrus cloud over both the warmer and colder parts of the region. Figure 11 shows the clear radiances inferred in the clear-sky compositing step; the bimodal VIS and IR distributions associated with the snow-covered and snow-free parts of the region are apparent. The final threshold results (Figs. 10e and 10j) show that the contrast of VIS and IR radiances between cloudy and clear is not large in this winter scene.

In summary, we find that in those regions where clouds cause a relatively large variation of the radiances, the combined IR space/time contrast tests successfully separate the radiance distribution mostly into cloudy and clear categories; the undecided category is much lower in population than the other two categories and has radiance distributions lying between the peaks of the other two distributions. The stricter tests for clear do miss some scenes that may represent clear conditions, shifting them to the undecided category, but some cloud contamination is also apparent. The resulting IR radiances are not altered much by this contamination on average. In more difficult circumstances, where clouds either do not alter the IR radiances very much or where cloudiness is unusually persistent, these tests still separate the extremes of the radiance distribution and indicate the "confusion" by much larger populations of undecided and mixed categories. Even in the very difficult marine stratus case (Fig. 9), the clear radiances approximate the correct clear IR radiances with only a small cold bias. More complex situations over land, even in winter with snow cover, seem to be separated relatively well; however, comparisons to other measurements provide a better evaluation of the algorithm for these cases (Rossow and Garder 1993).

c. *Clear-sky composites*

The radiance compositing procedure is based on the premise that the part of the IR and VIS radiance distributions produced by clear conditions (determined primarily by surface variations at these wavelengths) have characteristic shapes described by the difference between the modal and extreme (maximum IR and minimum VIS) radiance values (Sèze and Rossow 1991a). The IR space/time contrast tests serve to

FIG. 15. Frequency distribution of (a) the separation by the VIS threshold test of VIS radiances into clear (solid), marginally cloudy (dashed), and cloudy (dotted), where the classifications by the IR threshold test are indicated by IR = CLR, IR = MARG, IR = CLD, and (b) the separation by the IR threshold test of IR radiances into clear, marginally cloudy, and cloudy, where the VIS classifications are indicated by VIS = CLR, VIS = MARG, VIS = CLD. Results are from the whole Meteosat region (Fig. 4a) for July 1983, separated into land and ocean areas.

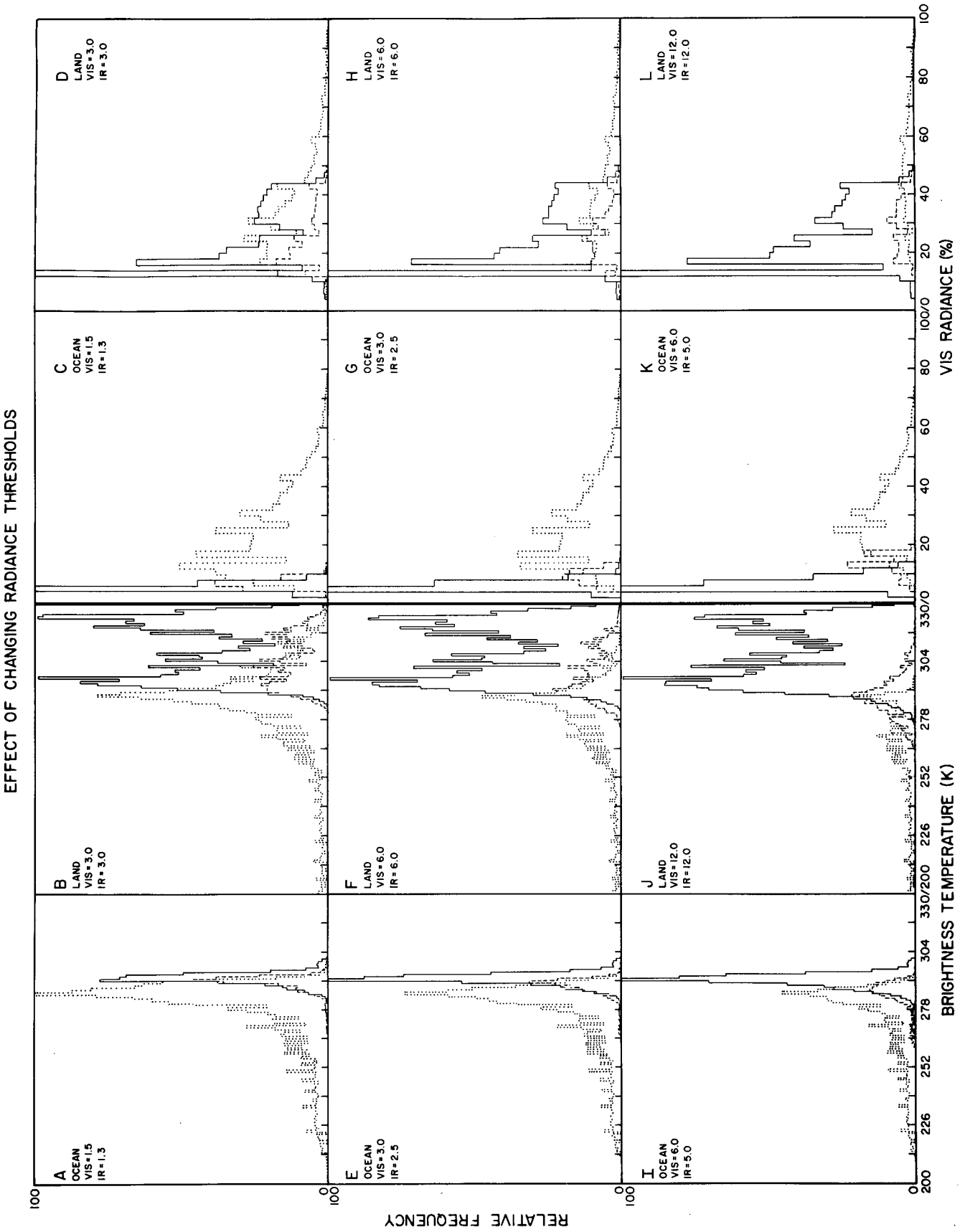
EFFECT OF CHANGING RADIANCE THRESHOLDS
A
OCEAN
VIS=1.5
IR=1.3
B
LAND
VIS=3.0
IR=3.0
C
OCEAN
VIS=1.5
IR=1.3
D
LAND
VIS=3.0
IR=3.0
E
OCEAN
VIS=3.0
IR=2.5
F
LAND
VIS=6.0
IR=6.0
G
OCEAN
VIS=3.0
IR=2.5
H
LAND
VIS=6.0
IR=6.0
I
OCEAN
VIS=6.0
IR=5.0
J
LAND
VIS=12.0
IR=12.0
K
OCEAN
VIS=6.0
IR=5.0
L
LAND
VIS=12.0
IR=12.0
RELATIVE FREQUENCY
100
0
200 226 252 278 304 330/200 226 252 278 304 330/0
100/0 80 60 40 20 0 20 40 60 80 100
BRIGHTNESS TEMPERATURE (K)
VIS RADIANCE (%)

eliminate the majority of cloudy scenes from the distribution, so that the average of the remaining values will be close to the modal value, if the distribution is narrow enough (Rossow et al. 1989b). The remaining cloud contamination does not alter clear IR radiance values too much, but further tests are made to detect shifts of the average IR radiances caused by contamination. The particular statistics used are, for IR (in terms of brightness temperatures), the average of the clear radiances from the IR space/time contrast tests over a short and long time period, $T_{AVG\text{-}ST}$ and $T_{AVG\text{-}LT}$, the maximum value for the same periods (without regard to the results of the IR space/time contrast tests), $T_{MAX\text{-}ST}$ and $T_{MAX\text{-}LT}$, and the number of clear scenes, N_{CLEAR}. For VIS (in terms of reflectances), the statistics are simply $R_{MIN\text{-}ST}$ and $R_{MIN\text{-}LT}$; however, here we use the behavior of R_{AVG} (the average reflectance of scenes labeled clear by the IR space/time contrast tests) to evaluate cloud contamination. We also use the quantities $T_{MAX}(R_{MIN})$ and $R_{MIN}(T_{MAX})$. The former is the maximum of the T values in a small area associated with the R_{MIN} for each scene and the latter has a corresponding meaning.

TABLE 9. Summary of cloud detection error assessments.

Section	Comments	Error estimate
4a	• Variations of temporal and spatial mode radiance values place limits on variability of clear radiances: should be less than threshold used	<5% bias
4b	• Number of mixed and undecided results indicates how well separated cloudy and clear radiances are: maximum cloud amount error	<10% random
4c	• Average differences in T_{AVG} and T_{MAX}, as well as in T_{MAX} and R_{MIN} values, suggest natural variability of clear radiances: should be smaller than thresholds	<5% random
4d	• Sensitivity of results to factor of 2 changes in threshold magnitude	±10% random
	• Amount of extra cloudiness detected by VIS channel (amount missed at night)	5%–10% negative bias

1) IR CLEAR-SKY COMPOSITE

Figure 12 shows a survey of the distribution over the GOES-EAST view (Fig. 4b) of T_{MAX} and R_{MIN} collected over 5-, 15-, and 30-day periods. Note that the variety of surface types and climates (e.g., moist–dry) produces very broad distributions of radiance extrema. Figures 12b, 12d, 12f, and 12h show the differences between the 30-day and shorter-term values, which are remarkably narrow considering the width of the distributions of T_{MAX} and R_{MIN} (Figs. 12a, 12c, 12e, and 12g). The distributions of T_{MAX} and R_{MIN} show a progressive warming and darkening, respectively, as the accumulation period increases (cf. Sèze and Rossow 1991a). That the 30-day minus 5-day T_{MAX} distribution is very similar to the 30-day minus 15-day T_{MAX} distribution, particularly over ocean (Figs. 12b and 12f), shows that the 5-day statistic already captures a good measure of clear-sky conditions for most locations; however, the R_{MIN} difference distributions show that some remaining contamination by low clouds is eliminated by changing from 5 days to 15 days. The key fact illustrated by Fig. 12 is that the differences among the T_{MAX} and R_{MIN} values are nearly the same over the whole domain; essentially identical results were obtained in a global survey. This and other results comparing the differences of T_{AVG} and R_{AVG} with T_{MAX} and R_{MIN}, respectively, demonstrate a nearly constant shape of the clear-sky radiance distributions (cf. Sèze and Rossow 1991a). Thus, in the clear-sky compositing procedure, the differences between $T_{MAX\text{-}LT}$ and $T_{MAX\text{-}ST}$ and T_{MAX} and T_{AVG} are useful for detecing cloud contamination. The increased detection of marine stratus clouds by the final IR threshold (Fig. 9) illustrates the success of this approach.

The assumed shape of the clear-sky IR radiance distribution is indicated by the magnitudes of the values of DEL1, DEL2, and DEL3 (Table 3). Table 5 shows the effects of reducing these values to half their standard values. The stricter tests force the compositing procedure to use $T_{MAX\text{-}ST}$ and $T_{MAX\text{-}LT}$ more frequently, but the main effect is that the smaller values of DEL2 and DEL3 lead to slightly warmer values of T_{CLR}. The associated R_{CLR} values hardly change and cloud amount increases by less than one percent. Notice, however, that the R_{CLR} values for regions 7, 12, 13, and 14 (cf. Fig. 4a), which are regions of persistent low-level cloudiness, still indicate significant cloud contamination, even with the stricter tests.

The constancy of the $(T_{MAX} - T_{AVG})$ and $(R_{AVG} - R_{MIN})$ histogram widths can be shown to be associated with clear conditions by plotting the average values of these differences against values of N_{CLEAR} (Fig. 13), which are determined from the IR space/time contrast tests. We expect cloud contamination to in-

FIG. 16. Frequency distribution of IR and VIS radiances over ocean and land areas in the Meteosat region (Fig. 4a) separated by the VIS/IR radiance threshold tests using values that are one-half the standard values (a–d), the standard values (e–h), and twice the standard values (i–l). The first two panels in each row show the separation of IR radiances over ocean and land and the second two show the separation of VIS radiances over ocean and land. Clear radiances are indicated by the solid lines, marginally cloudy radiances by the dashed lines, and cloudy radiances by the dotted lines.

crease the width of the distributions in Figs. 12b, 12d, 12f, and 12h, thereby increasing the average values of $(T_{MAX} - T_{AVG})$ and $(R_{AVG} - R_{MIN})$. Over land, the value of $(T_{MAX} - T_{AVG})$ increases gradually as N_{CLEAR} decreases until reaching a sharp change at $N_{CLEAR} = 3$–5 (upper part of Fig. 13). The nearly constant value of $(R_{AVG} - R_{MIN})$ (lower part of Fig. 13) shows, however, that this increase is not associated with decreasing cloud contamination. Examination of the geographic distribution of the differences shows that the increase in $(T_{MAX} - T_{AVG})$ is due to increasing surface temperature variability over particular land areas rather than cloud contamination. As we go from large N_{CLEAR} to small N_{CLEAR}, the values of $(T_{MAX} - T_{AVG})$ shift from cloud-free desert regions to cloudier midlatitude regions. Thus over land, we emphasize the test on the value of N_{CLEAR} over land to decide on the reliability of the statistics obtained from the IR space/time contrast tests.

The value $(T_{MAX} - T_{AVG})$ over oceans shows an increase at $N_{CLEAR} = 2$–4, but the behavior of $(R_{AVG} - R_{MIN})$ indicates significant cloud contamination can occur out to $N_{CLEAR} \approx 10$. This problem is caused by areas with very persistent low-level clouds, which do not bias the value of T_{CLR} much but are difficult to detect in IR. Thus, a test on N_{CLEAR} is not as good an indicator of cloud contamination over all ocean areas; so over oceans we emphasize the test $(T_{MAX\text{-}LT} - T_{MAX\text{-}ST}) \leq$ DEL1 (cf. Fig. 2a).

A test of the sensitivity of the cloud detection results to changing the value of minimum N_{CLEAR} produces an effect similar to use of smaller or larger DEL values in that too strict a test (requiring much larger values of minimum N_{CLEAR}) shifts too many scenes toward long-term statistics; whereas elimination of the test (requiring only one value) causes cloud contamination of the clear radiances. Figure 13 shows that the minimum values of N_{CLEAR} needed to remove cloud contamination are between 3 and 10; however, Table 6 shows that, although there are significant changes in the branching ratio from short term to long term, the actual effect on the value of T_{CLR} and cloud amount caused by varying the minimum N_{CLEAR} from 2 to 9 is quite small. We have found that the less strict test that we use ($N_{CLEAR} \geq 3$) still detects contamination, even over ocean, as judged from VIS tests, and that the stricter test, suggested by Fig. 13, does not improve results significantly.

We summarize the advantages of the clear-sky compositing scheme by comparing the results obtained with a simpler algorithm; namely, $T_{CLR} = T_{MAX}$. Table 7 shows that such an approach would not be beneficial for global results. That the net effect of using $T_{CLR} = T_{MAX}$ (5 days) is to decrease clouds, more over oceans than land, demonstrates the negative effects associated with cloud cover persistence and the improvement that is made by using long-term information. However, simple substitution of T_{MAX} values from longer time periods, while generally increasing the detected cloud amount, produces more false than real detections (here we have used the VIS threshold to split the "new" clouds into clear and cloudy parts). Our more complicated procedure attempts to determine the relative amount of cloudiness and only uses clear-sky statistics from longer time periods as cloudiness increases. The success of this approach is shown by the fraction of the time that long-term statistics are used as a function of monthly mean cloud amount (Fig. 14); the arrows indicate the values of monthly mean cloud amount above which the probability is high for a particular 15-day (ocean) or 5-day (land) time subperiod to be mostly cloudy.

2) VIS CLEAR-SKY COMPOSITE

The stability of surface VIS reflectances over time, as reflected in the generally narrow distributions of $R_{AVG} - R_{MIN}$ shown in Fig. 12 (also see Sèze and Rossow 1991a), makes VIS clear-sky compositing simpler (Fig. 2b). The primary issues are to avoid biases in use of $R_{MIN\text{-}LT}$ in regions where the time variations are larger and to detect contamination by unusually persistent clouds. Examples of the former are snow and sea ice regions, where there are significant differences between short-term and long-term R_{MIN} values. Although the use of a 5-day R_{MIN} over snow-covered land may not guarantee that clear conditions are encountered, the histograms in Figs. 10 and 11 show that the cloud effects on VIS radiances in such locations are weak. Thus, even if the particular radiance value may represent partially cloudy conditions, it is still a good estimate of the actual clear radiance value. An example of the latter situation occurs in the Congo, where persistent hazes/fogs over the rain forest are only discernable by comparing its R_{MIN} values to those for other rain forests.

d. Radiance threshold sensitivity

Table 8 shows how scenes in each category from the space/time contrast tests are finally classified by the radiance threshold tests. That a larger fraction of clear scenes from the space/time contrast tests are classified as cloudy over ocean indicates more frequent occurrences of very low-level clouds over ocean than over land that are obvious to a VIS threshold test. Overall, the undecided category is generally classified as clear by the final threshold, confirming the supposition that these scenes are generally similar to the clear scenes from the space/time contrast tests (cf. Figs. 6–10). Mixed scenes are generally classified as cloudy by the threshold test.

To check the consistency of the independent threshold classifications by VIS and IR, we show in Fig. 15a the VIS radiance distributions, first classified as clear, marginal, and cloudy by the IR threshold, and then

classified by the VIS threshold. The complementary results for the IR radiances are shown in Fig. 15b. Panels A and D in Fig. 15a show that only a small amount of low-level cloudiness is missed by the IR threshold, whereas the same panels in Fig. 15b show somewhat more, very thin cirrus missed by the VIS threshold over land (primarily over the brighter deserts). The presence of low-level cloudiness is suggested by the overlap of IR radiance distributions for scenes classified as cloudy by the VIS threshold and both cloudy and clear by the IR threshold (panels C and F in Fig. 15b), particularly over oceans. Likewise the presence of very thin cirrus is indicated by overlapping VIS radiance distributions for scenes classified as cloudy by the IR threshold and both cloudy and clear by the VIS threshold (panels C and F in Fig. 15a), particularly over land. Figure 15a shows that clouds marginally detected by the IR threshold (about 10%–15% of the cases) are a combination of thin cirrus missed by the VIS threshold and low-level clouds more easily detected by the VIS threshold. Likewise, Fig. 15b shows a similar mixture for clouds marginally detected by the VIS threshold (about 5%–10% of the cases). These results support the conclusion that most of the marginally cloudy category actually represents cloudy scenes.

We test the overall sensitivity of the cloud detection results to the selected radiance threshold values (Table 4) by showing in Fig. 16 how the VIS/IR radiance distributions in the Meteosat view (Fig. 4a) are divided into cloudy, marginal, and clear categories using threshold values one-half the standard, standard, and twice the standard values. These results suggest that the behavior of the algorithm is reasonable and plausible, in that smaller thresholds appear to label as cloudy more of the scenes with radiances similar to the clear part of the distributions and larger thresholds label as clear more of the scenes with radiances similar to the cloudy part of the distribution. The key result is that although the cloud amount changes by about $\pm 10\%$ with changing threshold magnitudes, the average values of the clear and cloudy radiances do not change very much. Thus, although cloud amount is sensitive to the threshold selected, the inferred properties of clouds and the surface are not very sensitive (cf. Rossow et al. 1989b).

5. Summary

The main points of this paper are as follows.

The primary assumption at the heart of the ISCCP cloud detection algorithm is that cloudy and clear scenes differ in the amount of radiance variability that they exhibit in space and/or time. The variety of situations encountered has been illustrated in Figs. 6–10 (cf. Sèze and Rossow 1991a) and the results of the space/time contrast tests shown.

Although all situations cannot be separated equally well by variability in the same wavelength (VIS or IR) or the same domain (space or time), the time variation test is generally more successful because the variability of the land and ocean surface properties generally produces less radiance variability than produced by clouds (Fig. 12). Nevertheless, a global cloud detection algorithm must employ tests for all wavelengths and domains to account for all combinations of cloud and surface types.

A secondary assumption used in the ISCCP cloud detection algorithm is that the warm/dark end of the IR/VIS radiance distributions is associated with clear conditions (Figs. 12 and 13), so that statistical tests over a range of space and time domains of the shape of this part of the radiance distribution can be used to improve the estimated clear radiance values (Figs. 6–10). This assumption is violated more frequently in polar regions, as discussed in Rossow and Garder (1993).

The final radiance threshold test labels as cloudy those scenes with radiance values that differ from the inferred clear values by more than their uncertainty. This is a "conservative" test in that clouds will be missed more often than falsely detected if the threshold magnitudes correctly represent the clear radiance uncertainties, including biases (Fig. 16).

Allowing test parameter values to vary with location (Tables 1–4) makes it possible to account for differences in the magnitude of radiance variations associated with different surface and cloud types, to allow changes in the relative importance of the different algorithm tests, and to account for variations in the uncertainty of the clear radiances determined by the natural variability of the surface and the contrast with cloudy radiances.

Table 9 summarizes estimates of cloud detection error from the sensitivity tests of the ISCCP cloud detection algorithm, showing the sections where they are discussed. These results suggest random errors of no more than 10% and regional bias errors of no more than 5%. In regions with more persistent cloud cover and in winter land areas and the polar regions, where the radiance contrast between cloudy and clear conditions is much smaller, cloud detection errors are larger (see Rossow and Garder 1993).

Acknowledgments. This work has benefited from discussions with a large number of colleagues over the years. We wish to thank participants in the algorithm intercomparison studies, particularly A. Arking, J. Coakley, M. Desbois, E. Harrison, P. Minnis, F. Mosher, E. Raschke, E. Ruprecht, G. Sèze, and E. Smith. We wish to highlight the contributions of G. Sèze, who worked with us on the crucial final designs; her work on time variations of the radiances was key to use of this concept in the cloud algorithm. We also thank B. Barkstrom, F. Bretherton, G. Gutman, A. Henderson-Sellers, T. Inoue, J. Key, J. London, R. Saunders, M. Schlesinger, A. Slingo, G. Stephens, L.

Stowe, and T. Vonder Haar for thoughtful comments and B. Wielicki and D. Wylie for an ongoing conversation about the meaning of "cloud." ISCCP is the first project of the World Climate Research Program. During organization and operations of ISCCP, P. Morel was director of the Joint Planning Staff for WCRP at WMO and T. Kaneshige (succeeded by S. Benedict) was the staff member responsible for coordinating ISCCP meetings and reports. The international project manager and source of our funding for ISCCP is Dr. Robert Schiffer (NASA). We thank A. Walker for suggested improvements to the paper. Drafting was done by L. Del Valle and word processing by C. Koizumi; we thank them for their excellent support.

APPENDIX

ISCCP data processing has been accomplished by the combined efforts of several institutions, which are listed here along with their representatives (in chronological order). The capture of original satellite datasets, quality checking, and their reduction by sampling are performed by the sector processing centers (SPC). For NOAA polar orbiters, the SPC is the National Oceanic and Atmospheric Administration (represented by G. Hunolt, H. Jacobowitz, H. Drahos, J. Gibson, M. Mignono, and K. Kidwell). For Meteosat, the SPC is the European Space Agency (ESA) (R. Saunders, B. Mason). For GOES-East, the SPC was the University of Wisconsin (R. Fox, D. Wylie) and is now the Atmospheric Environment Service (AES) of Canada (S. Woronko, S. Lapczak, F. Bowkett, D. McKay, Y. Durocher). For GOES-West, the SPC is Colorado State University (CSU) (G. G. Campbell). The University of Wisconsin also serves as a backup to AES and CSU and produces special datasets for related research. For GMS, the SPC is the Japan Meteorological Agency (JMA) (A. Kurosaki, I. Kubota, T. Nuomi, K. Shuto). Normalization of geostationary satellite radiances to those measured by the polar orbiters is performed by the Satellite Calibration Center (SCC) at the Centre de Meteorologie Spatiale in France (N. Beriot, G. Therry, Y. Desormeaux). The ISCCP datasets are produced and analyzed at the Global Processing Center at NASA Goddard Institute for Space Studies (processing group led by E. Kinsella and A. Walker). NOAA serves as the International Central Archives (ICA) for ISCCP. In addition to the data center representatives, membership of the JSC Working Group on Data Management for ISCCP (now for all WCRP radiation projects) included T. Vonder Haar and E. Raschke; ex-officio members representing the WCRP are S. Benedict (who succeeded T. Kaneshige) and R. Schiffer (project manager).

REFERENCES

Arking, A., and J. D. Childs, 1985: Retrieval of cloud cover parameters from multispectral satellite measurements. *J. Climate Appl. Meteor.*, **24**, 322–333.

Brest, C. L., and W. B. Rossow, 1992: Radiometric calibration and monitoring of NOAA AVHRR data for ISCCP. *Int. J. Remote Sens.*, **13**, 235–273.

Coakley, J. A., and F. P. Bretherton, 1982: Cloud cover from high-resolution scanner data: Detecting and allowing for partially filled fields of view. *J. Geophys. Res.*, **87**, 4917–4932.

——, and D. G. Baldwin, 1984: Towards the objective analysis of clouds from satellite imagery. *J. Climate Appl. Meteor.*, **23**, 1065–1099.

Cotton, W. R., and R. A. Anthes, 1989: *Storm and Cloud Dynamics.* International. Geophys. Ser. 44., Academic Press, 883 pp.

Desbois, M., and G. Sèze, 1984: Use of space and time sampling to produce representative satellite cloud classifications. *Ann. Geophys.*, **2**, 599–606.

Desormeaux, Y., W. B. Rossow, C. L. Brest, and G. G. Campbell, 1993: Normalization and calibration of geostationary satellite radiances for ISCCP. *J. Atmos. Oceanic Tech.*, **10**, 304–325.

Gutman, G., D. Tarpley, and G. Ohring, 1987: Cloud screening for determination of land surface characteristics in a reduced resolution satellite data set. *Int. J. Remote Sens.*, **8**, 859–870.

Hartmann, D. L., V. Ramanathan, A. Berroir, and G. E. Hunt, 1986: Earth radiation budget data and climate research. *Rev. Geophys.*, **24**, 439–468.

Hobbs, P. V., 1974: *Ice Physics.* Oxford, 671 pp.

House, F. B., A. Gruber, G. E. Hunt, and A. T. Mecherikunnel, 1986: History of satellite missions and measurements of the earth radiation budget (1957–1984). *Rev. Geophys.*, **24**, 357–378.

Hughes, 1984: Global cloud climatologies: A historical review. *J. Climate Appl. Meteor.*, **23**, 724–751.

Key, J., and R. G. Barry, 1989: Cloud cover analysis with Arctic AVHRR data. 1. Cloud detection. *J. Geophys. Res.*, **94**, 8521–8535.

Kuo, K. S., R. M. Welch, and S. K. Sengupta, 1988: Structural and textural characteristics of cirrus clouds observed using high spatial resolution LANDSAT imagery. *J. Appl. Meteor.*, **27**, 1242–1260.

London, J., 1957: A study of atmospheric heat balance. Final Report. Contract AF19(122)-165, *AFCRC-TR-57-287,* College of Engineering, New York University, 99 pp. [Available from University of Colorado, Boulder, CO.]

Lorenz, E. N., 1967: *The Nature and Theory of the General Circulation of the Atmosphere.* WMO-No. 218. TP. 115. World Meteorological Organization, 161 pp.

Manabe, S., and R. F. Strickler, 1964: Thermal equilibrium of the atmosphere with a convective adjustment. *J. Atmos. Sci.*, **21**, 361–385.

Masaki, G. T., 1976: The Wolf Plotting and Contouring Package. GSFC Computer Program Lib. #A00227, Computer Sciences Corporation, NASA Goddard Space Flight Center, Greenbelt, MD, 187 pp.

Mason, B. J., 1971: *The Physics of Clouds.* (2nd edition). Oxford, 671 pp.

Matthews, E., 1983: Global vegetation and land use: New high resolution data bases for climate studies. *J. Climate Appl. Meteor.*, **22**, 474–487.

——, 1984: Prescription of land-surface boundary conditions in GISS GCM II: A simple method based on high-resolution vegetation data bases. NASA Tech. Memo. #86096.

——, and W. B. Rossow, 1987: Regional and seasonal variations of surface reflectance from satellite observations at 0.6 μm. *J. Climate Appl. Meteor.*, **26**, 170–202.

Minnis, P., and E. F. Harrison, 1984: Diurnal variability of regional cloud and clear sky radiative parameters derived from GOES data. Part I: Analysis method. *J. Climate Appl. Meteor.*, **23**, 993–1011.

Peixoto, J. P., and A. H. Oort, 1992: *Physics of Climate.* American Institute of Physics, 520 pp.

Pinty, B., and G. Szejwach, 1985: A new technique for inferring surface albedo from satellite observations. *J. Climate Appl. Meteor.*, **24**, 741–750.

Pruppacher, H. R., and J. D. Klett, 1980: *Microphysics of Clouds and Precipitation.* D. Reidel, ed., Dordrecht, 714 pp.

Reynolds, D. W., and T. H. Vonder Haar, 1977: A bi-spectral method for cloud parameter determination. *Mon. Wea. Rev.*, **105,** 446–457.

Rossow, W. B., 1989: Measuring cloud properties from space: A review. *J. Climate,* **2,** 201–213.

——, and A. A. Lacis, 1990: Global, seasonal cloud variations from satellite radiance measurements. Part II: Cloud properties and radiative effects. *J. Climate,* **3,** 1204–1253.

——, and R. A. Schiffer, 1991: ISCCP cloud data products. *Bull. Amer. Meteor. Soc.,* **72,** 2–20.

——, and L. C. Garder, 1993: Validation of ISCCP cloud detections. *J. Climate,* **6,** 2370–2393.

——, F. Mosher, E. Kinsella, A. Arking, M. Desbois, E. Harrison, P. Minnis, E. Ruprecht, G. Sèze, C. Simmer, and E. Smith, 1985: ISCCP cloud algorithm intercomparison. *J. Climate Appl. Meteor.,* **24,** 877–903.

——, E. Kinsella, A. Wolf, and L. Garder, 1987: International Satellite Cloud Climatology Project (ISCCP) Description of Reduced Resolution Radiance Data. WMO/TD No. 58. World Meteorological Organization, 143 pp. [Available from World Meteorological Organization, Geneva, Switzerland.]

——, C. L. Brest, and L. C. Garder, 1989a: Global, seasonal surface variations from satellite radiance measurements. *J. Climate,* **2,** 214–247.

——, L. C. Garder, and A. A. Lacis, 1989b: Global, seasonal cloud variations from satellite radiance measurements. Part I: Sensitivity of analysis. *J. Climate,* **2,** 419–458.

——, L. C. Garder, P. J. Lu, and A. W. Walker, 1991: International Satellite Cloud Climatology Project (ISCCP) Documentation of Cloud Data. *WMO/TD-No. 266 (Revised).* World Meteorological Organization, Geneva, 76+ pp. [Available from World Meteorological Organization, Geneva, Switzerland.]

——, A. W. Walker, and L. C. Garder, 1993: Comparison of ISCCP and other cloud amounts. *J. Climate,* **6,** 2394–2418.

Saunders, R. W., 1986: An automated scheme for removal of cloud contamination from AVHRR radiances over western Europe. *Int. J. Remote Sens.,* **7,** 867–886.

——, and Kriebel, 1988: An improved method for detecting clear sky and cloudy radiances from AVHRR data. *Int. J. Remote Sens.,* **9,** 123–150.

Schiffer, R. A., and W. B. Rossow, 1983: The International Satellite Cloud Climatology Project (ISCCP): The first project of the World Climate Research Program. *Bull. Amer. Meteor. Soc.,* **64,** 779–784.

——, ——, 1985: ISCCP global radiance data set: A new resource for climate research. *Bull. Amer. Meteor. Soc.,* **66,** 1498–1505.

Sèze, G., and M. Desbois, 1987: Cloud cover analysis from satellite imagery using spatial and temporal characteristics of the data. *J. Climate Appl. Meteor.,* **26,** 287–303.

——, and W. B. Rossow, 1991a: Time-cumulated visible and infrared radiance histograms used as descriptors of surface and cloud variations. *Int. J. Remote Sens.,* **12,** 877–920.

——, and ——, 1991b: Effects of satellite data resolution on measuring the space-time variations of surfaces and clouds. *Int. J. Remote Sens.,* **12,** 921–952.

Shenk, W. F., and R. J. Curran, 1973: A multi-spectral technique to determine sea surface temperature using *NIMBUS 2* data. *J. Appl. Meteor.,* **12,** 1213–1216.

Simmer, C., E. Raschke, and E. Ruprecht, 1982: A method for determination of cloud properties from two-dimensional histograms. *Ann. Meteor.,* **18,** 130–132.

Stowe, L. L., C. G. Wellemeyer, T. F. Eck, H. Y. M. Yeh, and the NIMBUS-7 Cloud Data Processing Team, 1988: NIMBUS-7 global cloud climatology. Part I: Algorithms and validation. *J. Climate,* **1,** 445–470.

Twomey, S., 1977: *Atmospheric Aerosols.* Elsevier Scientific, 302 pp.

Warren, S. G., C. J. Hahn, J. London, R. M. Chervin, and R. L. Jenne, 1986: Global distribution of total cloud and cloud type amounts over land. NCAR Tech. Note TN-273+STR/DOE Tech. Rep. ER/60085-H1, 29 pp. + 200 maps. [NTIS number DE87-00-6903]

——, ——, ——, ——, and ——, 1988: Global distribution of total cloud and cloud type amounts over the ocean. NCAR Tech. Note TN-317+STR/DOE Tech. Rep. ER-0406, 42 pp. + 170 maps. [NTIS number DE90-00-3187]

Welch, R. M., K. S. Kuo, B. A. Wielicki, S. K. Sengupta, and L. Parker, 1988: Marine stratocumulus cloud fields off the coast of southern California observed using LANDSAT imagery. Part I: Structural characteristics. *J. Appl. Meteor.,* **27,** 341–362.

Whitlock, C. H., W. F. Staylor, G. Smith, R. Levin, R. Frouin, C. Gautier, P. M. Teillet, P. N. Slater, Y. J. Kaufman, B. N. Holben, W. B. Rossow, C. L. Brest, and S. R. LeCroy, 1990: AVHRR and VISSR satellite instrument calibration results for both cirrus and marine stratocumulus IFO periods. FIRE Science Report 1988. NASA CP-3083, 141–145 [Available from World Meteorological Organization, Geneva, Switzerland.]

Wielicki, B. A., and L. Parker, 1992: On the determination of cloud cover from satellite sensors: The effect of sensor spatial resolution. *J. Geophys. Res.,* **97,** 12 799–12 823.